Carcinogenesis, 2015, Vol. 36, No. 2, 192–201

doi:10.1093/carcin/bgu238
Advance Access publication December 4, 2014
Original Manuscript

ORIGINAL MANUSCRIPT

Identification of coexistence of DNA methylation and H3K27me3 specifically in cancer cells as a promising target for epigenetic therapy

Hideyuki Takeshima, Mika Wakabayashi, Naoko Hattori, Satoshi Yamashita and Toshikazu Ushijima*

Division of Epigenomics, National Cancer Center Research Institute, 5-1-1 Tsukiji, Chuo-ku, Tokyo 104-0045, Japan

*To whom correspondence should be addressed. Tel: +81 3 3547 5240; Fax: +81 3 5565 1753; Email: tushijim@ncc.go.jp

Abstract

Alterations of epigenetic modifications are promising targets for cancer therapy, and several epigenetic drugs are now being clinically utilized. At the same time, individual epigenetic modifications have physiological functions in normal cells, and cancer cell specificity is considered difficult to achieve using a drug against a single epigenetic modification. To overcome this limitation, a combination of epigenetic modifications specifically or preferentially present in cancer cells is a candidate target. In this study, we aimed to demonstrate (i) the presence of a cancer cell-specific combination of epigenetic modifications by focusing on DNA methylation and trimethylation of histone H3 lysine 27 (H3K27me3) and (ii) the therapeutic efficacy of a combination of DNA demethylation and EZH2 inhibition. Analyses of DNA methylation and H3K27me3 in human colon, breast and prostate cancer cell lines revealed that 24.7±4.1% of DNA methylated genes had both DNA methylation and H3K27me3 (dual modification) in cancer cells, while it was 11.8±7.1% in normal cells. Combined treatment with a DNA demethylating agent, 5-aza-2′-deoxycytidine (5-aza-dC) and an EZH2 inhibitor, GSK126, induced marked re-expression of genes with the dual modification, including known tumor-suppressor genes such as *IGFBP7* and *SFRP1*, and showed an additive inhibitory effect on growth of cancer cells *in vitro*. Finally, an *in vivo* combined treatment with 5-aza-dC and GSK126 inhibited growth of xenograft tumors more efficiently than a single treatment with 5-aza-dC. These results showed that the dual modification exists specifically in cancer cells and is a promising target for cancer cell-specific epigenetic therapy.

Introduction

Epigenetic alterations, including aberrant DNA methylation and alterations in histone modifications, are frequently present in human cancers (1,2), and are promising targets for cancer therapy (3,4). Currently, DNA demethylating agents, 5-azacytidine (azacitidine) and 5-aza-2′-deoxycytidine (decitabine; 5-aza-dC), are clinically being utilized for patients with myelodysplastic syndromes (5–7), and histone deacetylase (HDAC) inhibitors, vorinostat and romidepsin, are utilized for patients with cutaneous T-cell lymphoma (8). Not only in hematological malignancies but also in solid tumors, multiple trials of these epigenetic drugs have been conducted, and the efficacy has been shown, at least in non-small cell lung cancers (9). In addition, inhibitors of various histone methyltransferases, such as DOT1L (EPZ004777), EZH2 (EI1, EPZ-6438 and GSK126) and G9a (BIX-01294), have been developed, and their efficacies have been demonstrated in preclinical studies (10–14).

Among the various epigenetic modifications, DNA methylation and trimethylation of histone H3 lysine 27 (H3K27me3) have critical roles in carcinogenesis. DNA methylation of promoter CpG islands (CGIs) is involved in the repression of tumor-suppressor genes, such as *BRCA1*, *CDKN2A* (p16) and *RASSF1A* genes (15–17). H3K27me3 is involved in the repression of tumor-suppressor genes, such as *CDH1* (E-cadherin) and *DKK1* (18,19), independently of DNA methylation (20). At the same time,

Received: March 8, 2014; **Revised:** November 6, 2014; **Accepted:** November 26, 2014

Abbreviations

5-Aza-dC	5-aza-2′-deoxycytidine
CGI	CpG island
HDAC	histone deacetylase
H3K27me3	trimethylation of histone H3 lysine 27
PBS	phosphate-buffered saline
TSS	transcription start site

individual epigenetic modifications, including DNA methylation and H3K27me3, have physiological functions in normal cells (21,22), such as repression of transposable elements and genes required for embryonic development and cellular differentiation (23,24). Therefore, cancer cell specificity is considered difficult to achieve using a drug against a single epigenetic modification.

To overcome this limitation, a combination of epigenetic modifications specifically or preferentially present in cancer cells is a potential target. As a candidate for such a combination, we here focused on DNA methylation and H3K27me3 because of their functional crosstalk during carcinogenesis. Namely, H3K27me3 in normal cells functions as a premark of aberrant DNA methylation induction in cancer cells and also in normal-appearing tissues exposed to chronic inflammation (25–30). Switching of repression by H3K27me3 to that by DNA methylation is frequently observed for various genes during carcinogenesis (31). Since DNA methylation and H3K27me3 exist in a mutually exclusive manner in embryonic stem cells and normal cells (32,33), a failure in switching may generate a cancer cell-specific combination of epigenetic modifications, DNA methylation and H3K27me3. Indeed, it was recently reported that a combination of DNA methylation and H3K27me3 is specifically present in cancer cells (34).

In this study, we will first confirm the cancer cell specificity of the combination of DNA methylation and H3K27me3. Then, to reveal the potential of this combination as a target for cancer cell-specific epigenetic therapy, we will show whether or not a combination of DNA demethylation and EZH2 inhibition is effective for (i) re-expression of genes with both DNA methylation and H3K27me3 and (ii) inhibition of cancer cell growth *in vitro* and *in vivo*.

Materials and methods

Cell lines and drug treatment

Human prostate cancer cell lines (Du145 and PC3), breast cancer cell lines (MCF7 and MDA-MB-231), colon cancer cell lines (HCT116 and RKO), a normal prostatic epithelial cell line (RWPE1) and normal human colon epithelial cells (FHC) were purchased from the American Type Culture Collection (Rockville, MD). Normal human mammary epithelial cells were purchased from Cambrex (East Rutherford, NJ).

PC3 and MCF7 were seeded on day 0, and were treated (i) with 5-aza-dC (Sigma–Aldrich, St. Louis, MO) and/or GSK126 (Active Biochem, Maplewood, NJ) and (ii) with 5-aza-dC and/or entinostat (ChemScene, Monmouth Junction, NJ) for 4 days. Cell numbers were counted on day 5, and the cells were harvested. For 5-aza-dC and GSK126, drug concentrations used in the combined treatment were determined based on the inhibitory effect on DNA methylation (5-aza-dC) or H3K27me3 (GSK126) (Supplementary Figures 1A and 2A is available at *Carcinogenesis* Online). The selected doses of 5-aza-dC showed inhibitory effects on cell growth similar to the neighboring doses (Supplementary Figure 1B is available at *Carcinogenesis* Online). The selected dose of GSK126 showed a mild inhibitory effect on cell growth (Supplementary Figure 2B is available at *Carcinogenesis* Online). For entinostat, drug concentration used in the combined treatment was determined based on the inhibitory effect on cell growth. The selected dose of entinostat showed a mild inhibitory effect on cell growth (Supplementary Figure 3 is available at *Carcinogenesis* Online).

Genomic DNA was extracted by the standard phenol/chloroform method, and was quantified using a Quant-iT PicoGreen dsDNA Assay Kit (Life Technologies, Carlsbad, CA). Total RNA was extracted from cancer cell lines and their normal counterpart cells using ISOGEN (Nippon Gene, Tokyo, Japan).

Analysis of DNA methylation

Genome-wide analysis of DNA methylation was performed using an Infinium HumanMethylation450 BeadChip array (Illumina, San Diego, CA) as described previously (35). The DNA methylation level of an individual probe (CpG site) was obtained as the β value that ranged from 0 (unmethylated) to 1 (fully methylated). A total of 482 421 CpG sites were assembled into 296 494 genomic blocks, collections of CpG sites which were classified by their locations from transcription start sites (TSSs) [TSS1500 (regions between 200 bp upstream and 1500 bp upstream from TSS), TSS200 (a 200-bp upstream region from TSS), 5′-UTR, the 1st exon, the gene body, 3′-UTR and an intergenic region] and their relative location against a CGI (N Shelf, N Shore, CGI, S Shore, S Shelf and non-CGI) (35). Among the 296 494 genomic blocks, 61 422 were located in CGIs and 7384 of them were located in TSS200 (TSS200 CGIs). Individual TSS200 CGIs contained 1–14 (average 3.5 ± 1.8) CpG sites, whose DNA methylation levels can be detected by a BeadChip array. The DNA methylation level of an individual TSS200 CGI (individual gene) was evaluated using the mean β value of all the CpG sites within an individual TSS200 CGI. Genes with β values of 0.9 or more and those of 0.2 or less were defined as methylated and unmethylated genes, respectively. Genes with β values of 0.2–0.9 were considered as partially methylated genes.

Gene-specific analysis of DNA methylation was performed by quantitative methylation-specific PCR and bisulfite sequencing. Quantitative methylation-specific PCR was performed using primers specific to methylated or unmethylated DNA (Supplementary Table 1 is available at *Carcinogenesis* Online) and DNA methylation levels were calculated as [number of methylated molecules/number of the total DNA molecules (methylated molecules + unmethylated molecules) × 100]. Bisulfite sequencing was performed using universal primers for methylated and unmethylated DNA sequences (Supplementary Table 2 is available at *Carcinogenesis* Online). The PCR product was cloned into pGEM-T Easy vector (Promega, Madison, WI), and sequenced using a DYEnamic ET Terminator Cycle Sequencing kit (GE Healthcare, Buckinghamshire, UK) and an ABI PRISM 310 sequencer (PE Biosystems, Foster City, CA).

Analysis of H3K27me3

Chromatin immunoprecipitation for H3K27me3 was performed as described previously (29). Briefly, 30 μg of chromatin extracted from cross-linked cells was immunoprecipitated using 2 μg of antibody against H3K27me3 (07-449, Millipore, Billerica, MA). Immunoprecipitated chromatin was treated with RNaseA and proteinase K, and DNA was recovered by phenol/chloroform extraction and isopropanol precipitation. The precipitated DNA was dissolved in 30 μl of 1× TE (10 mM Tris–HCl, pH 8.0, 1 mM ethylenediaminetetraacetic acid).

Genome-wide analysis of H3K27me3 was performed using a human CGI oligonucleotide microarray (Agilent technologies, Santa Clara, CA) as described previously (29). H3K27me3 levels (Bound signal/Input signal) of individual genes were evaluated using genomic blocks used for DNA methylation analysis (by a BeadChip array). CGI microarray probes located within 100 bp from any BeadChip array probes in a genomic block were assigned to the genomic block (Supplementary Figure 4 is available at *Carcinogenesis* Online). The position of a CGI microarray probe was defined by the center position of a probe. The H3K27me3 level of an individual genomic block was evaluated using the mean H3K27me3 level of all the probes assigned to a genomic block. Genomic blocks whose H3K27me3 levels were 1.5 or more were defined as those with H3K27me3.

Analysis of H3K27me3 levels of individual genes was performed by ChIP-quantitative PCR as described previously (29) using primers listed in Supplementary Table 3 is available at *Carcinogenesis* Online. Analysis of DNA methylation of chromatin immunoprecipitated DNA was performed using 19 of 30 μl of immunoprecipitated DNA.

Analysis of gene expression

Genome-wide analysis of gene expression was performed using a SurePrint G3 Human GE Microarray 8×60K v2 (Agilent Technologies). From 200 ng

of total RNA, Cy3-labeled cRNA was synthesized using a Low Input Quick Amp Labeling Kit (Agilent Technologies) and 600 ng of labeled cRNA was fragmented and hybridized to a microarray. The microarray was scanned with an Agilent G2565BA microarray scanner (Agilent Technologies). The scanned data were processed using Feature Extraction Ver.10.7 software (Agilent Technologies), and analyzed using GeneSpring Ver.12.5 software (Agilent Technologies). The signal intensity of each probe was normalized so that the 75th percentile of signal intensity of all the probes would be 1.0. Mean signal intensity of all the probes within a gene was used as its expression level, and genes with signal intensities of 0.5 or more were considered to be expressed. Analysis of gene expression levels of individual genes was performed by quantitative RT-PCR as described previously (29) using primers listed in Supplementary Table 4 is available at *Carcinogenesis* Online.

Immunofluorescence

Cells were fixed with 4% formaldehyde and permeabilized by 1% Triton X-100 in 1× phosphate-buffered saline (PBS) (–). The cells were incubated in blocking buffer [1% bovine serum albumin in 1× PBS (–)], and then incubated with rabbit polyclonal antibody against H3K27me3 (1:1000; 07-449; Millipore) and mouse monoclonal antibody against histone H3 (1:1000; 300–34783; Wako, Tokyo, Japan). After washing with 1× PBS (–), cells were incubated with Alexa Fluor 594-conjugated goat anti-rabbit IgG (1:1000, Life Technologies) and Alexa Fluor 488-conjugated goat anti-mouse IgG (1:1000, Life Technologies). After washing with 1× PBS (–), coverslips were mounted using ProLong Gold antifade reagent with DAPI (Life Technologies). Fluorescence of stained cells was detected using a BZ-9000 microscope system (Keyence, Osaka, Japan).

Western blotting

Proteins in total cell lysate were separated by sodium dodecyl sulfate–polyacrylamide gel electrophoresis, and were transferred to a polyvinylidene difluoride membrane (Millipore). H3K27me3, histone H3 and EZH2 were detected using rabbit polyclonal antibody against H3K27me3 (1:1000; 07-449; Millipore), rabbit polyclonal antibody against histone H3 (1:5000; ab1791; Abcam, Cambridge, UK) and mouse monoclonal antibody against EZH2 (1:1000; 3147S; Cell Signaling Technology, Danvers, MA), respectively. Protein bands were quantified by using ImageJ 1.47v software.

Xenograft tumor formation assay in nude mice

PC3 cells (1.5×10^6 cells) were inoculated subcutaneously into 6-week-old male nude mice (BALB/cAJc1-nu/nu; CLEA Japan, Tokyo, Japan). 5-Aza-dC (0.2 mg/kg) and/or GSK126 (10 or 15 mg/kg) were intraperitoneally administrated three times per week. The length and width of tumors were measured using calipers and the tumor volume was calculated as [(length × width^2) × 0.5]. After 8 weeks, tumors were collected for the measurement of tumor weights, and total blood was collected for the analysis of the number of leukocytes, erythrocytes and platelets. All the animal experiments were approved by the Committee for Ethics in Animal Experimentation at the National Cancer Center.

Statistical analysis

The differences in H3K27me3 levels were evaluated by the Mann–Whitney U-test. The differences in cell growth were evaluated by the Student's t-test.

Gene ontology analysis

Gene ontology analysis was performed by DAVID bioinformatics resources (36,37) as described previously (29). The enrichment of genes in a biological process was analyzed by comparing a fraction of genes with an ontology among genes with gain (or loss) of H3K27me3 in cancer cells with that among all the genes with TSS200 CGIs.

Results

Increase of genes with both DNA methylation and H3K27me3 in cancer cells

DNA methylation status was compared between cancer cell lines and their normal counterpart cells in the colon, mammary glands, and prostate for 61 422 genomic blocks with CGIs. Bimodal distribution of DNA methylation levels was observed in both cancer cell lines and normal cells, but the number of methylated blocks was larger in cancer cell lines than in normal cells (Figure 1A). When the analysis was limited to 7384 TSS200 CGIs, the six cancer cell lines had methylation of 238–969 genes while normal cells had that of only 55–75 genes (Supplementary Table 5 is available at *Carcinogenesis* Online).

Then, H3K27me3 status was compared between cancer cell lines and normal cells. The numbers of genomic blocks (Figure 1B) and TSS200 CGIs (Supplementary Table 5 is available at *Carcinogenesis* Online) with H3K27me3 were similar between cancer (743–1165 TSS200 CGIs) and normal cells (576–973 TSS200 CGIs). When the changes of H3K27me3 status were analyzed, 331–645 and 254–554 TSS200 CGIs showed gain and loss, respectively, of H3K27me3 in cancer cells (Supplementary Table 6 is available at *Carcinogenesis* Online). Genes with gain of H3K27me3 tended to have gene functions related to cell communication and cell–cell signaling. In contrast, genes with loss of H3K27me3 tended to have gene functions related to development (Supplementary Table 7 is available at *Carcinogenesis* Online).

Overlap between genes with DNA methylation and those with H3K27me3 was then analyzed. In cancer cell lines, 24.7 ± 4.1% of methylated genes (49–248 genes) had both DNA methylation and H3K27me3 (dual modification). On the other hand, in normal cells, only 11.8 ± 7.1% of DNA methylated genes (4–12 genes) had the dual modification (Figure 1C). Among the genes with the dual modification, known tumor-suppressor genes, such as *IGFBP7* and *SFRP1* (38–40), were present (Supplementary Table 8 is available at *Carcinogenesis* Online). These results showed that the fraction of genes with the dual modification was increased in cancer cells compared with their normal counterpart cells.

The existence of DNA methylation and H3K27me3 on the same DNA molecules

The existence of DNA methylation and H3K27me3 on the same DNA molecules was analyzed in two cancer cell lines, PC3 and MCF7, by bisulfite sequencing of chromatin immunoprecipitated DNA (32,41). First, higher H3K27me3 levels were confirmed in the genes with the dual modification, *CNN3*, *SFRP1* and *SLC6A15*, than in housekeeping genes, *EEF1A1* and *GAPDH* (Figure 2A). Then, the DNA methylation status of the DNA molecules immunoprecipitated by anti-H3K27me3 antibody was analyzed. All the DNA molecules sequenced were densely methylated at promoter CGIs of these genes (Figure 2B). The result showed that DNA methylation and H3K27me3 coexisted on the same DNA molecules.

High H3K27me3 levels in normal cells for genes with the dual modification

DNA methylation and H3K27me3 status in normal counterpart cells were analyzed for genes with the dual modification and genes with only DNA methylation. H3K27me3 was present in normal cells for 54.6 ± 14.4% (20–150 genes) of genes with the dual modification in cancer cell lines and for 28.1 ± 7.3% (34–266 genes) of genes with only DNA methylation (Supplementary Table 9 is available at *Carcinogenesis* Online). When the H3K27me3 level was analyzed, it was significantly higher in genes with the dual modification than in genes with only DNA methylation (Figure 3). Neither DNA methylation nor H3K27me3 was present in normal cells for 29.9 ± 17.4% (4–104 genes) of genes with the dual modification in cancer cell lines and for 37.0 ± 16.8% (20–363 genes) of genes with only DNA methylation (Supplementary

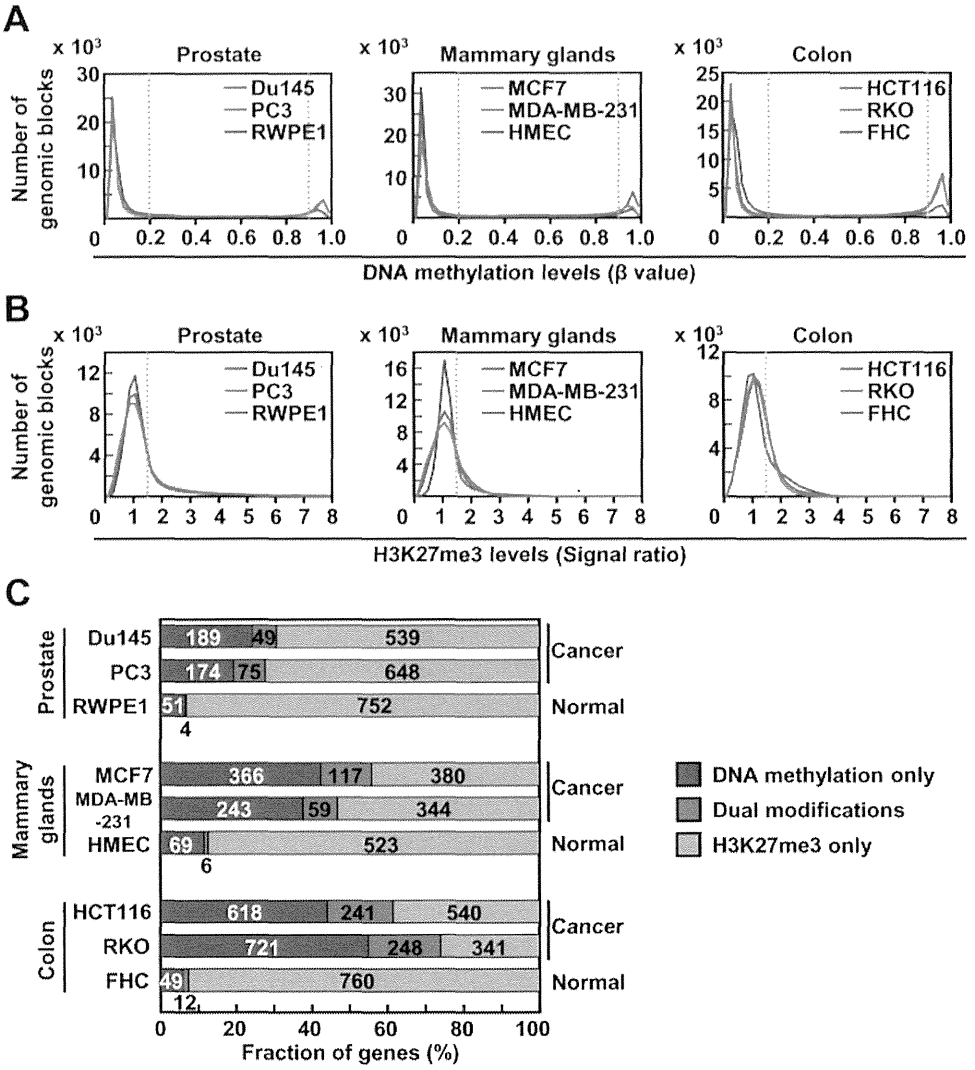

Figure 1. Increase of genes with DNA methylation and H3K27me3 (dual modification) in cancer cells. (**A**) Distribution of DNA methylation levels of 61 422 genomic blocks with CGIs. The number of methylated blocks was larger in cancer cell lines (Du145, PC3, MCF7, MDA-MB-231, HCT116 and RKO) than in their normal counterpart cells (RWPE1, HMEC and FHC). (**B**) Distribution of H3K27me3 levels of 56 523 genomic blocks with CGIs. The distribution of H3K27me3 levels was similar among cancer cell lines in each tissue. (**C**) Overlap of genes with DNA methylation and those with H3K27me3. The fraction of genes with the dual modification was increased in cancer cell lines compared with their normal counterpart cells.

Table 9 is available at *Carcinogenesis* Online). These results showed that genes with the dual modification frequently had high H3K27me3 levels in normal counterpart cells.

The repressive effect of the dual modification on gene expression

To analyze the effect of the dual modification on gene expression, the expression levels of the genes with the dual modification were compared with (i) those of genes with only DNA methylation, (ii) those of genes with only H3K27me3 and (iii) those of genes without DNA methylation or H3K27me3. The genes with the dual modification had the lowest expression levels, along with the genes with only DNA methylation, in all the four cancer cell lines (Figure 4A).

Characteristics of the genes with the dual modification and the resultant gene silencing were then examined. To this end, from the genes with the dual modification, we isolated genes that had neither DNA methylation nor H3K27me3 and were expressed in normal counterpart cells (Supplementary Table 9 is available at *Carcinogenesis* Online). This group of genes, except for *SLC6A12* (in MCF7) and *SPSB4* (in MDA-MB-231), was repressed to almost undetectable levels in cancer cell lines (Figure 4B). Well-established tumor-suppressor genes, such as *IGFBP7* and *SFRP1*, were present among this group of genes. These results showed that the dual modification was involved in the repression of genes expressed in normal cells, including tumor-suppressor genes.

Efficient re-expression by combination of DNA demethylation and EZH2 inhibition

Re-expression of genes with the dual modification by a combined treatment with a DNA demethylating agent, 5-aza-dC and an EZH2 inhibitor, GSK126, was attempted (Figure 5A). Genes with the dual modification, such as *IGFBP7*, *SFRP1* and *SLC6A15*, were re-expressed more efficiently by the combined treatment than by a single treatment with 5-aza-dC or GSK126 (Figure 5B and C; Supplementary Figure 5 is available at *Carcinogenesis* Online). In contrast, the effect of combined treatment was not observed

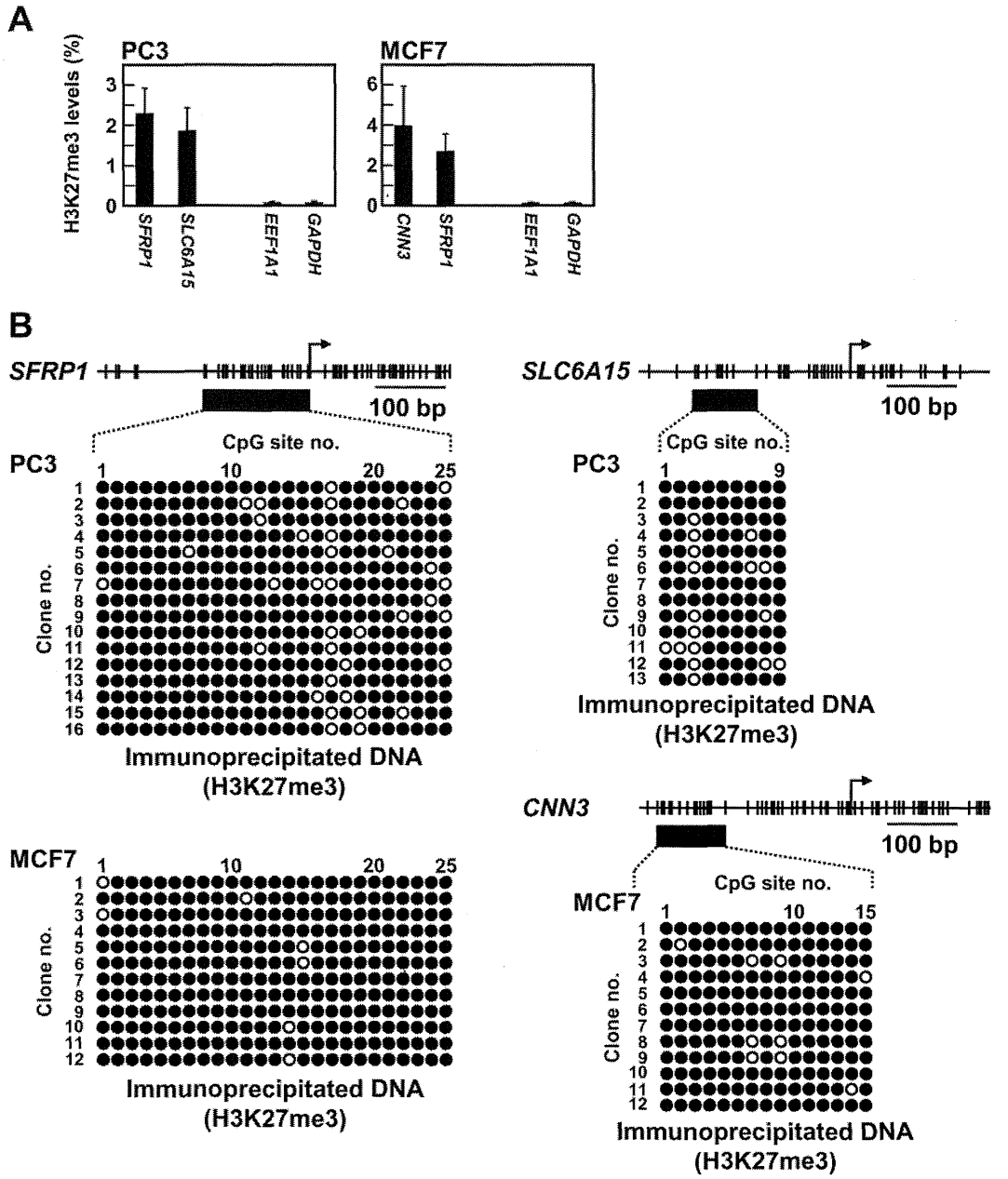

Figure 2. The coexistence of DNA methylation and H3K27me3 on the same DNA molecules. (**A**) H3K27me3 levels of genes with the dual modification. H3K27me3 levels were higher in the genes with the dual modification, *SFRP1*, *SLC6A15* and *CNN3*, than in housekeeping genes, *EEF1A1* and *GAPDH*. (**B**) Bisulfite sequencing of DNA molecules immunoprecipitated by anti-H3K27me3 antibody. All the DNA molecules were densely methylated for *SFRP1* (PC3 and MCF7), *SLC6A15* (PC3) and CNN3 (MCF7). Closed circle, methylated CpG site; open circle, unmethylated CpG site; vertical bar, CpG site; and arrow, TSS.

for genes with only DNA methylation (Figure 5B; Supplementary Figure 6 is available at *Carcinogenesis* Online) and genes with only H3K27me3 (Figure 5C; Supplementary Figure 7 is available at *Carcinogenesis* Online). Then, re-expression was confirmed in a genome-wide manner. Genes with the dual modification were re-expressed more efficiently by the combined treatment (Supplementary Figure 8 is available at *Carcinogenesis* Online). At the same time, even among the genes that had neither DNA methylation nor H3K27me3, 2-fold or more of upregulation was also observed (nonspecific changes) (Supplementary Figure 9 is available at *Carcinogenesis* Online).

The decrease of H3K27me3 level by a single treatment with GSK126 or by the combined treatment was confirmed in PC3 and MCF7 cell lines (Figure 5D–F; Supplementary Figure 2A is available at *Carcinogenesis* Online), but the EZH2 level was not changed (Figure 5E and F). These results showed that the combined treatment with a DNA demethylating agent and an EZH2 inhibitor was useful for re-expression of genes with the dual modification.

Additive inhibitory effect of the combination on cancer cell growth

First, the effect of the combined treatment with 5-aza-dC and GSK126 on growth of two cancer cell lines, PC3 and MCF7, was analyzed *in vitro* (Figure 6A and B). A single treatment with 5-aza-dC decreased growth of PC3 and MCF7 to 29.9 and 65.6%,

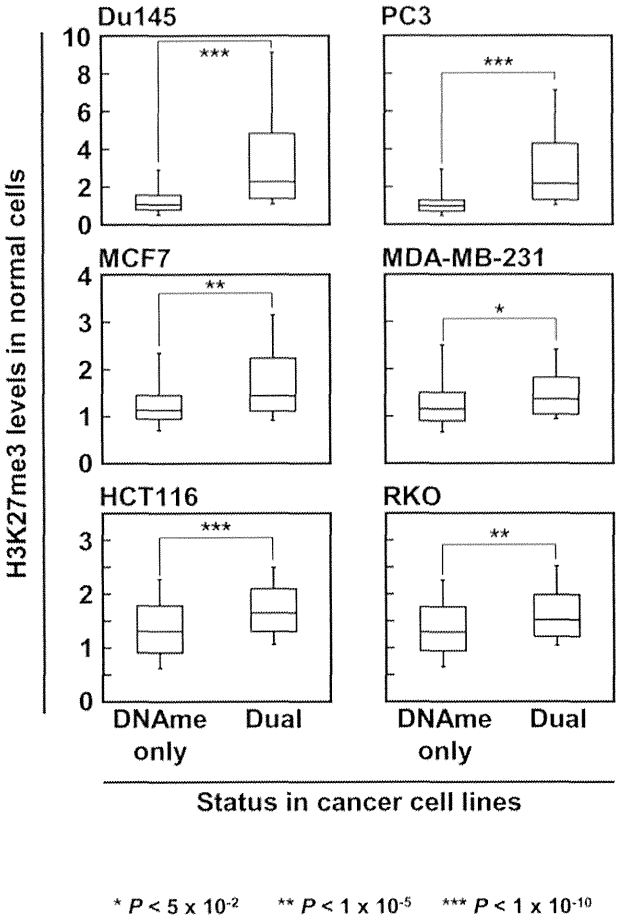

Figure 3. *High H3K27me3 levels in normal cells of genes with the dual modification in cancer cells.* H3K27me3 levels in normal cells were analyzed for genes with the dual modification and those with only DNA methylation in cancer cells. Genes with the dual modification had significantly higher levels of H3K27me3 than genes with only DNA methylation. The significance of difference was evaluated by the Mann–Whitney *U*-test ($^{*}P \leq 5\times10^{-2}$, $^{**}P \leq 1\times10^{-5}$, $^{***}P \leq 1\times10^{-10}$).

respectively, of untreated cells. A single treatment with GSK126 also decreased growth of PC3 and MCF7 to 76.7 and 42.9%, respectively, of untreated cells. The combined treatment with 5-aza-dC and GSK126 decreased growth of PC3 and MCF7 to 20.3 and 24.8%, respectively, of untreated cells.

Then, to compare these inhibitory effects with the combined treatment whose therapeutic efficacy was shown in a clinical trial (9), the effect of the combined treatment with 5-aza-dC and HDAC inhibitor, entinostat, was also analyzed (Supplementary Figure 10 is available at *Carcinogenesis* Online). A single treatment with entinostat decreased growth of PC3 and MCF7 to 66.9 and 42.7%, respectively, of untreated cells. The combined treatment with 5-aza-dC and entinostat decreased growth of PC3 and MCF7 to 18.5 and 30.8%, respectively, of untreated cells. These results showed that the combined treatment with a DNA demethylating agent and an EZH2 inhibitor had the additive inhibitory effect on growth of cancer cells, and the efficacy was comparable with that by the combined treatment with 5-aza-dC and entinostat.

Inhibitory effect of the combination on xenograft tumors

The effect of the combined treatment with 5-aza-dC and GSK126 on growth of PC3 xenograft tumors was analyzed. The combined treatment with 5-aza-dC and GSK126 inhibited growth of xenograft tumors (Figure 6C–E). In contrast, a single treatment with GSK126 had no inhibitory effect on growth of xenograft tumors, and that with 5-aza-dC could inhibit growth of six of eight xenografts. As for the side effects of the combined treatment, we did not observe significant changes of weights (Supplementary Figure 11A is available at *Carcinogenesis* Online). However, we observed a decrease in the numbers of leukocytes and erythrocytes and an increase in the number of platelets. The degree of these side effects was similar to those by a single treatment with 5-aza-dC (Supplementary Figure 11B is available at *Carcinogenesis* Online). These results showed that the combined treatment with 5-aza-dC and GSK126 inhibited growth of xenograft tumors more efficiently than a single treatment with 5-aza-dC.

Discussion

The combination of DNA demethylation and EZH2 inhibition had an additive inhibitory effect on cancer cell growth *in vitro*, and the efficacy was comparable with that by the combined treatment with 5-aza-dC and entinostat. The combined treatment also inhibited growth of xenograft tumors more efficiently than a single treatment with 5-aza-dC. This suggested that the cancer cell-specific dual modification is a promising target for cancer cell-specific epigenetic therapy. The effect of the combined treatment can be enhanced by (i) selecting DNA demethylating agents and EZH2 inhibitors suitable for combined treatment and (ii) optimizing the drug concentrations for the combination. Further to the increasing specificity for the dual modification, its reader proteins, if any, are ideal targets. The strategy of targeting a reader protein itself has been successful for histone acetylation, using inhibitors such as JQ1 and RVX-208, and was demonstrated to be effective in preclinical studies (42,43). Therefore, once reader proteins of the dual modification are identified, it might be possible to develop cancer cell-specific epigenetic therapy.

The presence of various physiological dual modifications, such as a combination of H3K4me3 and H3K27me3 (bivalent modification), has been reported (44). In this study, a cancer cell-specific combination of DNA methylation and H3K27me3 was used as a potential target for cancer cell-specific epigenetic therapy. However, genes with DNA methylation and H3K27me3 were also observed in normal cells although their number was extremely small, compared with that in cancer cells. In cancer cells, various epigenetic modifiers, such as DOT1L and EP300, are known to be dysregulated and their target modifications are altered (45,46). Therefore, the comparison of combinations of these epigenetic modifications between cancer cells and their normal counterpart cells might lead to identification of more combinations with cancer cell specificity.

Several known tumor-suppressor genes, such as *IGFBP7* and *SFRP1* (38–40), were among the genes with the dual modification. *IGFBP7* is known to be involved in the inhibition of the BRAF-MEK-ERK signaling pathway and also in the induction of cellular senescence and apoptosis (40). Repression of *IGFBP7* is critical for development of melanoma with BRAF V600E mutation (40). *SFRP1* is known as a negative regulator of the WNT signaling pathway, and repression of *SFRP1* leads to the activation of the WNT signaling pathway (47,48). The combination of DNA demethylation and EZH2 inhibition could induce re-expression of these genes. In addition to such an epigenetic effect, it is

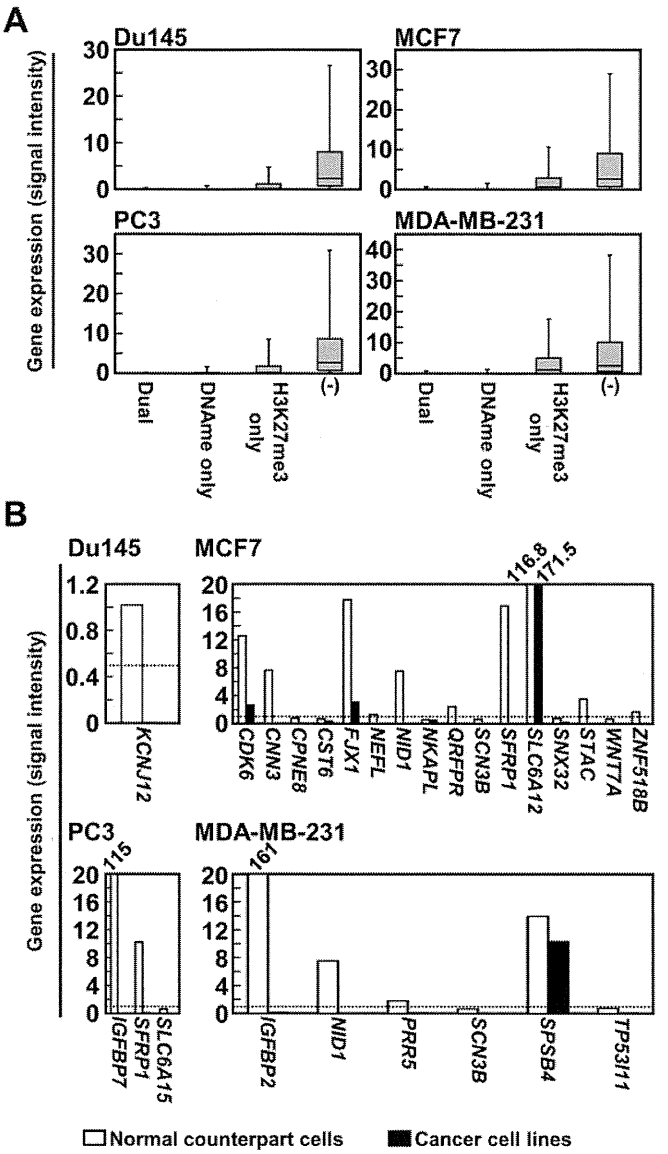

Figure 4. Repressive effect of the dual modification on gene expression. (**A**) Comparison of expression levels among four groups of genes–genes with the dual modification, those with only DNA methylation, those with only H3K27me3 and those without either. The genes with the dual modification had the lowest expression levels, along with those with only DNA methylation. (**B**) Repression of genes expressed in normal cells by the dual modification. From the genes with the dual modification, genes that had neither DNA methylation nor H3K27me3 and were expressed in normal counterpart cells were isolated. Expression levels were compared between cancer cell lines (black) and normal cells (white). Most of these genes were repressed to almost undetectable levels in cancer cell lines.

known that treatment with GSK126 induces both cytostatic and cytotoxic responses in lymphoma cell lines (13). Therefore, the therapeutic effect of the combined treatment was considered to be not only through the epigenetic effect but also through cytostatic and cytotoxic responses.

Mechanistically, in embryonic stem cells and normal cells, DNA methylation and H3K27me3 exist in a mutually exclusive manner (32,33). This is considered to be due to the inhibitory effect of DNA methylation on PRC2 recruitment (49). In contrast, in immortalized and transformed cells, the inhibitory effect of DNA methylation on PRC2 recruitment is known to be disrupted (33), and such disruption during carcinogenesis might be a possible mechanism of the preferential existence of the dual modification in cancer cells.

SLC6A12 and *SPSB4* were not repressed by the dual modification in cancer cells. As for the possible reasons, these genes might have been transcribed from TSSs different from the TSSs that had the dual modification. TSSs of a gene can vary from tissue to tissue depending upon genes (50), and a TSS in the database is not always accurate. It was also considered that only one allele of the gene had the dual modification in cancer cells and that the other allele was transcribed.

Combined treatment with 5-aza-dC and GSK126 induced marked re-expression of some genes with the dual modification, such as *CNN3*, *IGFBP7*, *NID1* and *SFRP1*, while not for the other genes, such as *CPNE8*, *NEFL* and *QRFPR*. To induce gene expression after the removal of repressive modifications, the presence of transcription factors required for the expression of individual genes is important. Therefore, it was considered that re-expression by the combined treatment might be dependent on the presence of sufficient amounts of such transcription factors in an analyzed cancer cell line.

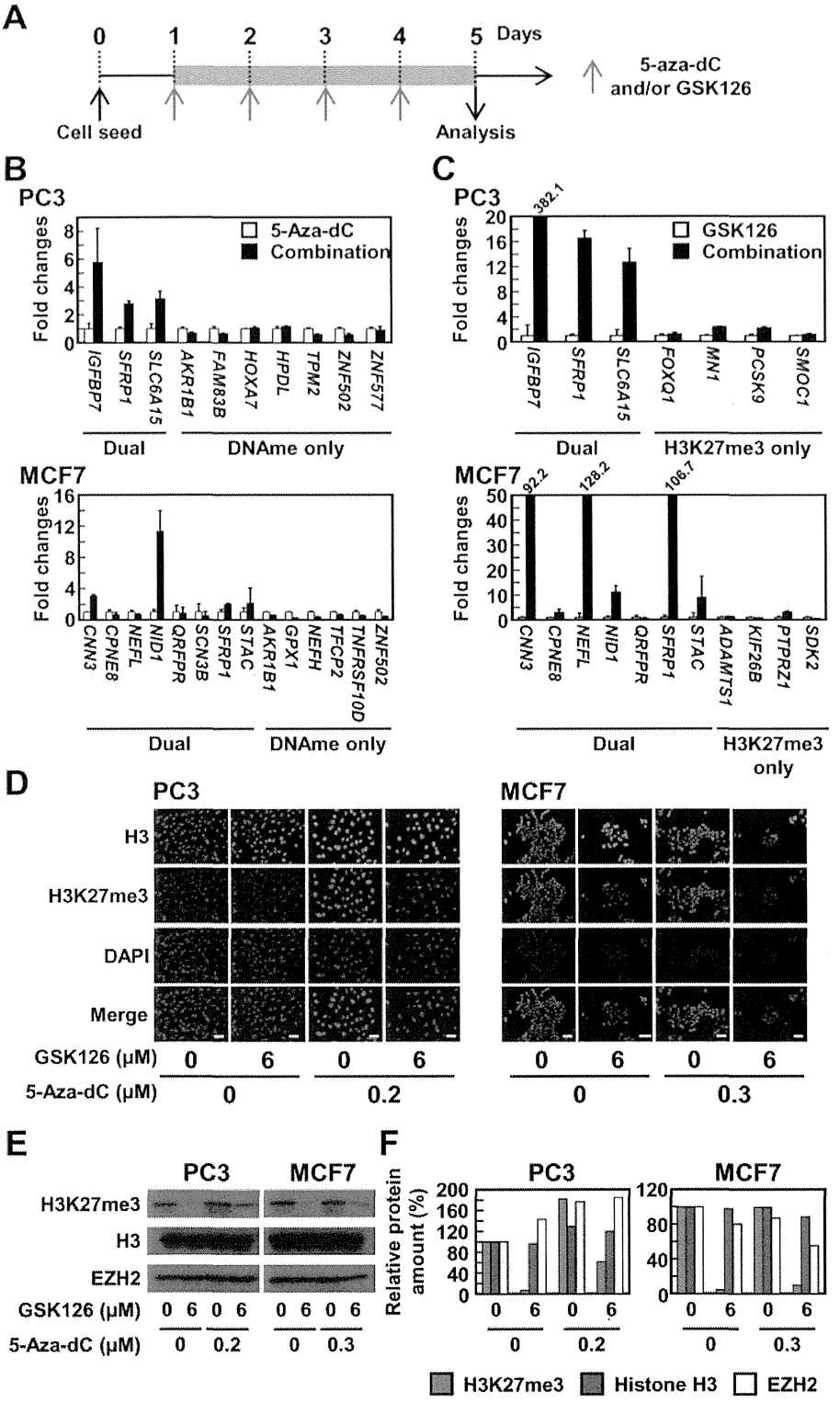

Figure 5. Efficient re-expression of genes with the dual modification by combination of DNA demethylation and EZH2 inhibition. (**A**) Experimental protocol of drug treatment. Two cancer cell lines, PC3 and MCF7, were treated with 5-aza-dC (0.2 μM for PC3 and 0.3 μM for MCF7) and/or GSK126 (6 μM) for 4 days, and harvested on day 5. (**B**), (**C**) Relative re-expression levels of genes with the dual modification and those with a single modification. The expression level of a gene in cells treated with the combination was normalized to that in cells treated with 5-aza-dC only (**B**) or to that in cells treated with GSK126 only (**C**). Genes with the dual modification were re-expressed more efficiently by the combined treatment than by a single treatment. (**D**) Immunofluorescence analysis of H3K27me3 in cells treated with 5-aza-dC and/or GSK126. The H3K27me3 level was decreased by a single treatment with GSK126 or by combined treatment with 5-aza-dC and GSK126. The scale bar represents 50 μm. (**E**), (**F**) Western blotting of H3K27me3 and EZH2 in cells treated with 5-aza-dC and/or GSK126. H3K27me3 levels were decreased by a single treatment with GSK126 and the combined treatment to 4.5–61.5% of those in untreated cells. EZH2 levels were not decreased by treatment with GSK126 as reported previously (13).

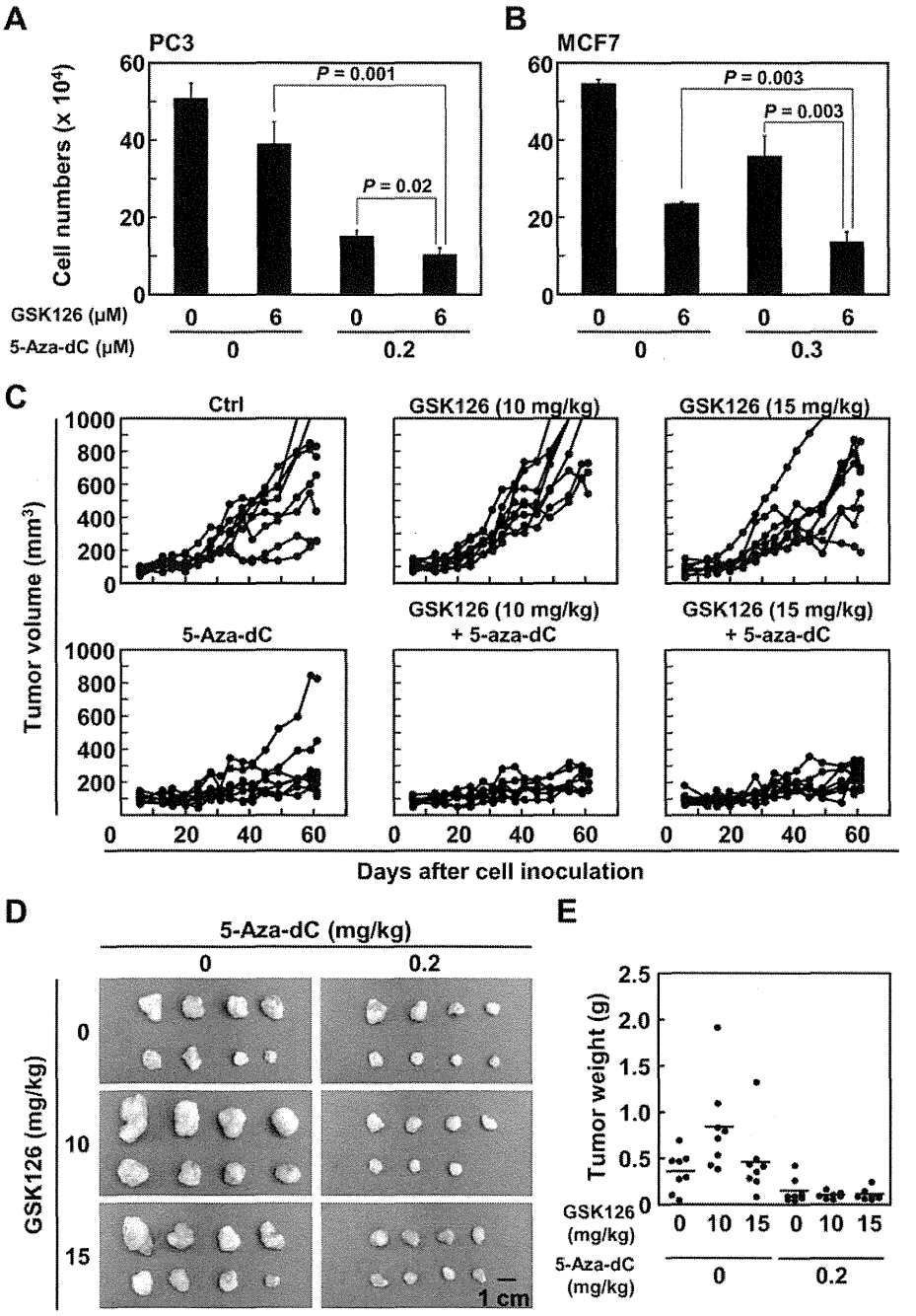

Figure 6. Therapeutic effects of the combination of DNA demethylation and EZH2 inhibition. (**A**), (**B**) Additive inhibitory effect of the combined treatment on cancer cell growth *in vitro*. Two cancer cell lines, PC3 and MCF7, were treated with the drugs according to the protocol shown in Figure 5A, and the cell number was counted on day 5. Additive inhibitory effect of the combination of DNA demethylation and EZH2 inhibition on cancer cell growth was observed in both PC3 (**A**) and MCF7 (**B**). The significance of difference was evaluated by the Student's t-test. (**C**), (**D**) and (**E**) The *in vivo* effect of the combined treatment. The combined treatment with 5-aza-dC and GSK126 reduced volume (**C**, **D**) and weight (**E**) of PC3 xenograft tumors more efficiently than a single treatment with 5-aza-dC.

In conclusion, a combination of DNA methylation and H3K27me3, which exists specifically in cancer cells, was considered to be a promising target for cancer cell-specific epigenetic therapy.

Supplementary material

Supplementary Table 1–9 and Figures 1–11 can be found at http://carcin.oxfordjournals.org/

Funding

Third-Term Comprehensive Cancer Control Strategy (H22-002) and Applied Research for Innovative Treatment of Cancer (H26-106) from the Ministry of Health, Labour and Welfare, Japan; Foundation for Promotion of Cancer Research in Japan; The National Cancer Center Research and Development Fund (26-A-15).

Conflict of Interest Statement: None declared.

References

1. Jones, P.A. et al. (2007) The epigenomics of cancer. Cell, 128, 683–692.
2. Laird, P.W. et al. (1996) The role of DNA methylation in cancer genetic and epigenetics. Annu. Rev. Genet., 30, 441–464.
3. Issa, J.P. (2007) DNA methylation as a therapeutic target in cancer. Clin. Cancer Res., 13, 1634–1637.
4. Mund, C. et al. (2010) Epigenetic cancer therapy: Proof of concept and remaining challenges. Bioessays, 32, 949–957.
5. DeWoskin, V.A. et al. (2013) The epigenetics pipeline. Nat. Rev. Drug Discov., 12, 661–662.
6. Kantarjian, H. et al. (2006) Decitabine improves patient outcomes in myelodysplastic syndromes: results of a phase III randomized study. Cancer, 106, 1794–1803.
7. Silverman, L.R. et al. (2002) Randomized controlled trial of azacitidine in patients with the myelodysplastic syndrome: a study of the cancer and leukemia group B. J. Clin. Oncol., 20, 2429–2440.
8. New, M. et al. (2012) HDAC inhibitor-based therapies: can we interpret the code? Mol. Oncol., 6, 637–656.
9. Juergens, R.A. et al. (2011) Combination epigenetic therapy has efficacy in patients with refractory advanced non-small cell lung cancer. Cancer Discov., 1, 598–607.
10. Daigle, S.R. et al. (2011) Selective killing of mixed lineage leukemia cells by a potent small-molecule DOT1L inhibitor. Cancer Cell, 20, 53–65.
11. Knutson, S.K. et al. (2013) Durable tumor regression in genetically altered malignant rhabdoid tumors by inhibition of methyltransferase EZH2. Proc. Natl. Acad. Sci. USA, 110, 7922–7927.
12. Kubicek, S. et al. (2007) Reversal of H3K9me2 by a small-molecule inhibitor for the G9a histone methyltransferase. Mol. Cell, 25, 473–481.
13. McCabe, M.T. et al. (2012) EZH2 inhibition as a therapeutic strategy for lymphoma with EZH2-activating mutations. Nature, 492, 108–112.
14. Qi, W. et al. (2012) Selective inhibition of Ezh2 by a small molecule inhibitor blocks tumor cells proliferation. Proc. Natl. Acad. Sci. USA, 109, 21360–21365.
15. Dammann, R. et al. (2000) Epigenetic inactivation of a RAS association domain family protein from the lung tumour suppressor locus 3p21.3. Nat. Genet., 25, 315–319.
16. Merlo, A. et al. (1995) 5' CpG island methylation is associated with transcriptional silencing of the tumour suppressor p16/CDKN2/MTS1 in human cancers. Nat. Med., 1, 686–692.
17. Rice, J.C. et al. (2000) Transcriptional repression of BRCA1 by aberrant cytosine methylation, histone hypoacetylation and chromatin condensation of the BRCA1 promoter. Nucleic Acids Res., 28, 3233–3239.
18. Fujii, S. et al. (2008) Enhancer of zeste homolog 2 downregulates E-cadherin by mediating histone H3 methylation in gastric cancer cells. Cancer Sci., 99, 738–746.
19. Osada, H. et al. (2008) Roles of achaete-scute homologue 1 in DKK1 and E-cadherin repression and neuroendocrine differentiation in lung cancer. Cancer Res., 68, 1647–1655.
20. Kondo, Y. et al. (2008) Gene silencing in cancer by histone H3 lysine 27 trimethylation independent of promoter DNA methylation. Nat. Genet., 40, 741–750.
21. Kouzarides, T. (2007) Chromatin modifications and their function. Cell, 128, 693–705.
22. Smith, Z.D. et al. (2013) DNA methylation: roles in mammalian development. Nat. Rev. Genet., 14, 204–220.
23. Di Croce, L. et al. (2013) Transcriptional regulation by Polycomb group proteins. Nat. Struct. Mol. Biol., 20, 1147–1155.
24. Levin, H.L. et al. (2011) Dynamic interactions between transposable elements and their hosts. Nat. Rev. Genet., 12, 615–627.
25. Hahn, M.A. et al. (2008) Methylation of polycomb target genes in intestinal cancer is mediated by inflammation. Cancer Res., 68, 10280–10289.
26. McCabe, M.T. et al. (2009) A multifactorial signature of DNA sequence and polycomb binding predicts aberrant CpG island methylation. Cancer Res., 69, 282–291.
27. Ohm, J.E. et al. (2007) A stem cell-like chromatin pattern may predispose tumor suppressor genes to DNA hypermethylation and heritable silencing. Nat. Genet., 39, 237–242.
28. Schlesinger, Y. et al. (2007) Polycomb-mediated methylation on Lys27 of histone H3 pre-marks genes for de novo methylation in cancer. Nat. Genet., 39, 232–236.
29. Takeshima, H. et al. (2009) The presence of RNA polymerase II, active or stalled, predicts epigenetic fate of promoter CpG islands. Genome Res., 19, 1974–1982.
30. Widschwendter, M. et al. (2007) Epigenetic stem cell signature in cancer. Nat. Genet., 39, 157–158.
31. Gal-Yam, E.N. et al. (2008) Frequent switching of Polycomb repressive marks and DNA hypermethylation in the PC3 prostate cancer cell line. Proc. Natl. Acad. Sci. USA, 105, 12979–12984.
32. Brinkman, A.B. et al. (2012) Sequential ChIP-bisulfite sequencing enables direct genome-scale investigation of chromatin and DNA methylation cross-talk. Genome Res., 22, 1128–1138.
33. Murphy, P.J. et al. (2013) Single-molecule analysis of combinatorial epigenomic states in normal and tumor cells. Proc. Natl. Acad. Sci. USA, 110, 7772–7777.
34. Gao, F. et al. (2014) Direct ChIP-bisulfite sequencing reveals a role of H3K27me3 mediating aberrant hypermethylation of promoter CpG islands in cancer cells. Genomics, 103, 204–210.
35. Kim, J.G. et al. (2013) Comprehensive DNA methylation and extensive mutation analyses reveal an association between the CpG island methylator phenotype and oncogenic mutations in gastric cancers. Cancer Lett., 330, 33–40.
36. Dennis, G. Jr et al. (2003) DAVID: Database for Annotation, Visualization, and Integrated Discovery. Genome Biol., 4, P3.
37. Huang da, W. et al. (2009) Systematic and integrative analysis of large gene lists using DAVID bioinformatics resources. Nat. Protoc., 4, 44–57.
38. Suzuki, H. et al. (2002) A genomic screen for genes upregulated by demethylation and histone deacetylase inhibition in human colorectal cancer. Nat. Genet., 31, 141–149.
39. Ugolini, F. et al. (2001) WNT pathway and mammary carcinogenesis: loss of expression of candidate tumor suppressor gene SFRP1 in most invasive carcinomas except of the medullary type. Oncogene, 20, 5810–5817.
40. Wajapeyee, N. et al. (2008) Oncogenic BRAF induces senescence and apoptosis through pathways mediated by the secreted protein IGFBP7. Cell, 132, 363–374.
41. Statham, A.L. et al. (2012) Bisulfite sequencing of chromatin immunoprecipitated DNA (BisChIP-seq) directly informs methylation status of histone-modified DNA. Genome Res., 22, 1120–1127.
42. Filippakopoulos, P. et al. (2010) Selective inhibition of BET bromodomains. Nature, 468, 1067–1073.
43. Picaud, S. et al. (2013) RVX-208, an inhibitor of BET transcriptional regulators with selectivity for the second bromodomain. Proc. Natl. Acad. Sci. USA, 110, 19754–19759.
44. Bernstein, B.E. et al. (2006) A bivalent chromatin structure marks key developmental genes in embryonic stem cells. Cell, 125, 315–326.
45. Füllgrabe, J. et al. (2011) Histone onco-modifications. Oncogene, 30, 3391–3403.
46. Plass, C. et al. (2013) Mutations in regulators of the epigenome and their connections to global chromatin patterns in cancer. Nat. Rev. Genet., 14, 765–780.
47. Jones, S.E. et al. (2002) Secreted Frizzled-related proteins: searching for relationships and patterns. Bioessays, 24, 811–820.
48. Nojima, M. et al. (2007) Frequent epigenetic inactivation of SFRP genes and constitutive activation of Wnt signaling in gastric cancer. Oncogene, 26, 4699–4713.
49. Bartke, T. et al. (2010) Nucleosome-interacting proteins regulated by DNA and histone methylation. Cell, 143, 470–484.
50. Carninci, P. et al. (2006) Genome-wide analysis of mammalian promoter architecture and evolution. Nat. Genet., 38, 626–635.

Cancer Science
Japanese Cancer Association JCA
Open Access

Nucleolar protein PES1 is a marker of neuroblastoma outcome and is associated with neuroblastoma differentiation

Masato Nakaguro,[1] Shinichi Kiyonari,[2] Satoshi Kishida,[2] Dongliang Cao,[2] Yuko Murakami-Tonami,[3] Hitoshi Ichikawa,[4] Ichiro Takeuchi,[5] Shigeo Nakamura[1] and Kenji Kadomatsu[2]

[1]Department of Pathology and Laboratory Medicine, Nagoya University Hospital, Nagoya; [2]Department of Biochemistry, Nagoya University Graduate School of Medicine, Nagoya; [3]Division of Molecular Oncology, Aichi Cancer Center Research Institute, Nagoya; [4]Division of Genetics, National Cancer Institute, Tokyo; [5]Department of Computer Science/Scientific and Engineering Simulation, Nagoya Institute of Technology, Nagoya, Japan

Key words
Differentiation, neuroblastoma, nucleolus, PES1, tumorigenesis

Correspondence
Kenji Kadomatsu, Department of Biochemistry, Nagoya University Graduate School of Medicine, 65 Tsurumai-cho, Showa-ku, Nagoya 466-8550, Japan.
Tel: +81-52-744-2059; Fax: +81-52-744-2060;
E-mail: kkadoma@med.nagoya-u.ac.jp

Funding Information
National Cancer Center of Japan; Ministry of Health, Labor and Welfare, Japan.

Received September 15, 2014; Revised December 1, 2014; Accepted December 20, 2014

Cancer Sci (2015)

doi: 10.1111/cas.12598

Neuroblastoma (NB) is a childhood malignant tumor that arises from precursor cells of the sympathetic nervous system. Spontaneous regression is a phenomenon unique to NBs and is caused by differentiation of tumor cells. PES1 is a multifunctional protein with roles in both neural development and ribosome biogenesis. Various kinds of models have revealed the significance of PES1 in neurodevelopment. However, the roles of PES1 in NB tumorigenesis and differentiation have remained unknown. Here we show that NB cases with *MYCN* amplification and clinically unfavorable stage (INSS stage 4) express higher levels of *PES1*. High *PES1* expression was associated with worse overall and relapse-free survival. In NB cell lines, *PES1* knockdown suppressed tumor cell growth and induced apoptosis. This growth inhibition was associated with the expression of NB differentiation markers. However, when the differentiation of NB cell lines was induced by the use of all-trans retinoic acid, there was a corresponding decrease in *PES1* expression. *Pes1* expression of tumorspheres originated from *MYCN* transgenic mice also diminished after the induction of differentiation with growth factors. We also reanalyzed the distribution of PES1 in the nucleolus. PES1 was localized in the dense fibrillar component, but not in the granular component of nucleoli. After treatment with the DNA-damaging agent camptothecin, this distribution was dramatically changed to diffuse nucleoplasmic. These data suggest that PES1 is a marker of NB outcome, that it regulates NB cell proliferation, and is associated with NB differentiation.

Neuroblastoma (NB) is the most common extracranial solid malignant tumor of childhood and is derived from precursor cells of the sympathetic nervous system.[1] Unlike in the case of other malignant tumors, a subset of patients with NBs show spontaneous regression without any treatment. This phenomenon is caused by differentiation and programmed cell death of tumor cells.[2] Differentiation induction and proliferation inhibition with 13-cis-retinoic acid is thus one of the effective therapies for high-risk NBs.[3] *MYCN* is a well-known driver gene of NBs. Twenty to thirty percent of NB cases show *MYCN* amplification and poor prognosis.[4] Although MYCN, which has a helix–loop–helix domain and belongs to the MYC family of transcription factors, activates the transcription of various kinds of growth signals, recent data show that MYCN is also required for the differentiation program.[5]

The gene *PES1* (and its zebrafish ortholog pes) is highly conserved from yeast to humans. *PES1* was originally identified in zebrafish in an insertional mutagenesis screen. *PES1* mutant embryos exhibited brains with reduced volumes and other developmental abnormalities.[6] *PES1* mutant overexpression disrupted oligodendrocyte development, oligodendrocyte migration, and axon extension.[7] In the developing *Xenopus laevis*, *pes1* is expressed in the migrating cranial neural crest cells. Inhibition of *pes1* using morpholino oligonucleotide caused neural crest migration impairment.[8] In developing mice, *Pes1* displayed a distinct spatial and temporal pattern of gene expression with high levels in the germinal zone and other specific brain regions that contain neural progenitor cells and postmitotic neurons.[9] In addition to these neurodevelopmental roles, PES1 plays a crucial part in ribosome neogenesis,[10,11] particularly in pre-ribosomal RNA (pre-rRNA) processing. In interphase cells, PES1 is localized in the nucleolus, an intranuclear body where ribosome neogenesis takes place.[12,13] Previous reports revealed that *PES1* was upregulated in glioblastoma, breast cancer, and head and neck squamous cell carcinoma.[9,14,15] The close relationship between ribosome biogenesis and carcinogenesis could be the reason for these upregulations. *PES1* knockdown has been shown to inhibit the proliferation and tumorigenicity of breast cancer cell lines.[16]

As described above, PES1 has two important roles, namely neural development and oncogenesis. These two key processes are themselves characteristics of NBs. Therefore, in the current study we investigated the relationship between PES1 and NBs. We show here that *PES1* is a prognostic marker of NBs and

regulates NB proliferation and apoptosis. Reduced *PES1* expression is associated with NB differentiation in NB cell lines and tumorsphere models. In addition, our analysis with confocal microscopy showed that PES1 is distributed in the dense fibrillar component (DFC) in the nucleolus, and its distribution is radically changed after treatment with the DNA-damaging agent camptothecin (CPT).

Materials and Methods

Mice. The *MYCN* transgenic (Tg) mice[17] were maintained in the animal facility at Nagoya University Graduate School of Medicine (Nagoya, Japan), where they were housed in a controlled environment and provided with standard nourishment and water. Normal ganglia and precancerous and tumor tissues from WT, hemizygous, and homozygous *MYCN* Tg mice were dissected and minced, and then total RNA was extracted. This study was approved by the Animal Care and Use Committee of Nagoya University Graduate School of Medicine.

Gene expression profiling. Gene expression profiling was carried out as previously described.[18] Samples were analyzed with a GeneChip Mouse Genome 430 2.0 array (Affymetrix, Santa Clara, CA, USA). The data have been deposited in the Gene Expression Omnibus database of NCBI (http://www.ncbi.nlm.nih.gov/geo) under the accession number GSE43419.

Human neuroblastoma tumor profile. Kaplan–Meier analysis of the prognosis of NB patients was performed on the R2 website (http://r2.amc.nl). The dataset was from the AMC cohort study of 88 NB patients (GSE16476). This dataset was profiled on the Affymetrix HGU133 plus2.0 platform and normalized using the MASS5.0 algorithm.

Cell culture. The human neuroblastoma cell lines NB39 and TNB1 were obtained from Riken Cell Bank (Tsukuba, Japan). SH-EP and *MYCN*-inducible SH-EP cell line (SH-EP^{MYCN}) cells were gifts from Dr. Schwab of the Division of Tumor Genetics, German Cancer Research Center (Heidelberg, Germany).[19] They were cultured with DMEM (D5796; Sigma-Aldrich, St. Louis, MO, USA) or RPMI-1640 (R8758; Sigma-Aldrich) or a mixture of some other media following the manufacturer's instructions. Induction of *MYCN* was regulated by removal of tetracycline (1 μg/mL). The media were supplied with 10% heat-inactivated FBS in an incubator with humidified air at 37°C with 5% CO_2. They were routinely authenticated on the basis of their viability, growth rate, and morphology by microscopic examination.

RNA interference. To deliver shRNA expression construct into NB cell lines, commercially available lentiviral shRNA vectors were used. Non-targeting shRNA (Sigma-Aldrich) and specific shRNAs for *PES1* (Open Biosystems, Little Chalfont, UK) were used. The shRNA sequences are listed in Table S1.

Plasmids and their transfection. Human *MYCN* construct was generated by PCR using the Gateway recombination system. *MYCN* construct was cloned into CSII-CMV-RfA-IRES-venus plasmid. This plasmid and CSII-CMV-venus control plasmid were kindly provided by Dr. Miyoshi of Riken. For producing lentiviral particles, HEK293T cells were co-transfected with shRNA plasmids or overexpression plasmid in addition to psPAX2 (Addgene, Cambridge, MA, USA) and pMD2.G (Addgene) plasmids using FuGENE HD reagent (Promega, Fitchburg, WI, USA) according to the manufacturer's instructions. The neuroblastoma cell lines were infected in the presence of 8 μg/mL polybrene (Sigma-Aldrich).

Quantitative RT-PCR. RNA extraction from cultured cells and tumorspheres, and quantitative RT-PCR were carried out as previously described.[20] Quantitative PCR analyses were carried out using an MX3000P or MX3005P real-time QPCR System (Agilent, Santa Clara, CA, USA). Quantitative PCR was carried out with ReverTra Ace (Toyobo, Osaka, Japan) and Thunderbird SYBR qPCR Mix (Toyobo). The relative expression levels were acquired according to the manufacturer's instructions. The primers used are listed in Table S2.

Immunocytochemistry. Immunocytochemistry was carried out as previously described using the following primary antibodies: rabbit anti-pescadillo (A300-902A; Bethyl Laboratories, Montgomery, TX, USA), mouse anti-pescadillo (#ab88543; Abcam, Cambridge, UK), rabbit anti-nucleolin (#ab22758; Abcam), mouse anti-phospho-histone H2AX (Ser139) (#05-636; Millipore, Billerica, MA, USA), and mouse anti-neuronal class III β-tubulin (Tuj1) (MMS-435p; Covance, Princeton, NJ, USA). Alexa Fluor 488-conjugated goat anti-rabbit IgG and Alexa Fluor 594-conjugated goat anti-mouse IgG were used as secondary antibodies. Hoechst 33258 was used to visualize nuclei.

Primary culture of tumorspheres from primary tumors of *MYCN* transgenic mice. The procedure was carried out as previously described.[21] Briefly, dissected tumor tissue was minced and digested with 0.25% trypsin (Sigma-Aldrich). To obtain tumorspheres from the primary tumors, the cells were suspended in DMEM/F12ham (Sigma-Aldrich) plus 10 ng/mL epidermal growth factor, 15 ng/mL basic fibroblast growth factor (Peprotech, Rocky Hill, NJ, USA), 2% B27 supplement, 1% penicillin/streptomycin (PS; Gibco, Waltham, MA, USA), 15% FBS (HyClone, Waltham, MA, USA), 1% non-essential amino acid, 1% sodium pyruvate, and 55 μM β-mercaptoethanol. Cells were cultured in a non-treated Petri dish in a 37°C, 5% CO_2 tissue culture incubator. To induce differentiation, spheres were collected and resuspended with medium containing DMEM/F12ham, 1% FBS, 2% B27 supplement, 1% sodium pyruvate, 10^3 U/mL leukemia inhibitory factor (LIF), and 1% PS. The spheres were seeded into a poly-D-lysine/laminin/fibronectin pre-coated dish. After 12 h the medium was changed to differentiation medium containing DMEM/F12 Ham, 1% FBS, 2% B27 supplement, 1% N2 supplement, 50 ng/mL nerve growth factor (NGF), 50 ng/mL neurotrophin-3 (NT3), and 1% PS.

TUNEL assay. The TUNEL assay was carried out using the APO-DIRECT kit (556381; BD Pharmingen, San Jose, CA, USA). Cell fixation and staining was carried out following the manufacturer's instructions. The cells were analyzed with BD FACSCalibur (BD Pharmingen) and BD CellQuest Pro software (BD Biosciences, San Jose, CA, USA).

Data analysis. Results are expressed as the mean ± SD. Their homoscedasticities were checked by the *f*-test. Statistical significance was evaluated with a two-tailed, unpaired Student's *t*-test.

Results

***PES1* expression increased with NB tumor development in *MYCN* Tg mouse model.** To examine the relationship between NB formation and *PES1* expression, we used a *MYCN* Tg mouse model.[17] In this model, human *MYCN* is overexpressed under the tyrosine hydroxylase promoter, which is active in migrating neural crest cells. At 2 weeks of age, the superior mesenteric ganglion (SMG) of WT mice and hemizygous or homozygous *MYCN* Tg mice are similar in size. However, compared to those of 2-week-old WT mice, the SMGs of 2-week-old homozygote *MYCN* Tg mice show accumulation of immature neuroblasts microscopically. These SMGs can be

regarded as "precancerous" or "hyperplastic" lesions.[18,20,22,23] Finally, at age 6–14 weeks, 100% (for homozygotes) or approximately 70% (hemizygotes) of Tg mice develop NB and die. Histology of tumors of both hemizygous and homozygous *MYCN* Tg mice are similar and equivalent to human neuroblastomas.[23] We first examined the expression profiles of the SMGs of 2-week-old WT mice, the SMGs of 2-week-old homozygous *MYCN* Tg mice, and the terminal tumors of 6-week-old hemizygous or homozygous *MYCN* Tg mice (GSE43419). The precancerous lesions (2-week-old homozygous MYCN Tg mice SMG) showed higher *Pes1* expression than the normal ganglia, and the terminal tumors of hemizygous or homozygous *MYCN* Tg mice showed even higher *Pes1* expression than the precancerous ganglia or WT ganglia (Fig. 1). This suggests that *Pes1* expression increased as the NBs grew in the *MYCN* Tg mouse model.

***PES1* expression associated with poor prognosis of NB.** We then investigated *PES1* expression in human NB cases. For this analysis we used the database from an AMC cohort study of 88 NB patients (GSE16476) and the R2 genomics analysis and visualization platform. Expression of *PES1* was significantly higher in the *MYCN*-amplified cases ($P = 6.9 \times 10^{-10}$; Fig. 2a). *MYCN* amplification has been associated with rapid disease progression and unfavorable prognosis.[4] As the *PES1* promotor region has an E-box, the MYCN binding sequence, we examined whether *MYCN* induction enhances *PES1* expression. *MYCN* induction in SH-EP^{MYCN},[19] SY5Y and SH-EP cell lines significantly increased *PES1* expression (Fig. S1). This result was consistent with Figure 2(a). Tumor stage is also an important prognostic factor of NBs. Neuroblastomas were previously classified based on the International Neuroblastoma Staging System (INSS).[24] Although this classification is widely accepted, in 2009, the International Neuroblastoma Risk Group proposed a new staging system.[25] Both classifications include the designations 4S or MS, in addition to 4 and M, which indicate metastatic diseases. The S is short for "special," and indeed the 4S and MS stages are unique to NBs. The 4S (or MS) cases show favorable prognosis and spontaneous regression in spite of multiple metastases of the skin, liver, or bone marrow. We investigated the *PES1* expression in each of the INSS stages using the same cohort. Stage 4 cases showed higher levels of *PES1* expression than stage 1–3 cases ($P = 0.008$; Fig. 2b). In addition, compared to stage 4S cases, stage four cases also showed significantly higher *PES1* expression ($P = 0.016$; Fig. 2b). The correlation of *PES1* expression with *MYCN* status or clinical stage raised the possibility that *PES1* might be a good prognostic marker. We therefore analyzed the prognostic value of *PES1* expression using Kaplan–Meier survival curves. High *PES1* expression was significantly associated with poorer overall survival ($P = 8.4 \times 10^{-5}$ after Bonferroni correction; Fig. 2c) and relapse-free survival ($P = 5.4 \times 10^{-3}$ after Bonferroni correction; Fig. 2d). Previous reports have indicated that malignant tumors express higher *PES1* levels than normal tissues or benign tumors in other types of cancers.[9,14–16,26] In line with previous findings, these results indicate that *PES1* expression is correlated with *MYCN* status and clinical stage, and that *PES1* is a prognostic marker of NBs.

***PES1* knockdown suppressed NB cell growth and induced apoptosis.** As NB cases with high *PES1* expression are associated with unfavorable prognosis, we next investigated the role of PES1 in NB cell lines. We knocked down *PES1* expression using two different shRNAs against human *PES1*. The shRNAs efficiently knocked down *PES1* expression at both the mRNA and protein level (Fig. 3a,b). Short hairpin RNAs suppressed the growth of both a *MYCN*-amplified cell line (NB39) and a *MYCN* non-amplified cell line (SH-EP) (Fig. 3c,d). We next carried out a TUNEL assay to examine whether these growth suppressions were caused by apoptosis. Compared to non-targeting shRNA, shRNAs against *PES1* dramatically increased the percentage of TUNEL-positive cells (Fig. 3e,f). These data suggest that *PES1* knockdown inhibited NB cell growth and this inhibition was caused by apoptosis.

As already described, tumor cell differentiation is both a characteristic and an important treatment strategy of NB.[3] Accordingly, we next investigated whether *PES1* knockdown causes the differentiation of NB cells. Differentiated cells possess more and longer neurites and express higher levels of differentiation markers (GAP43, RET).[27] Although *PES1* knockdown did not induce clear increase in neurite outgrowth

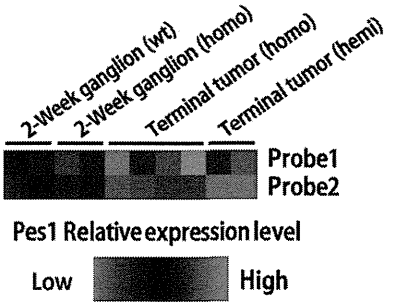

Fig. 1. *Pes1* expression in a neuroblastoma mice model. Results of a microarray analysis of the relative expression levels of *Pes1* in superior mesenteric ganglia of wild-type mice (wt), 2-week homozygous *MYCN* transgenic (Tg) mice (precancerous lesions) and terminal tumors (hemizygous and homozygous *MYCN* Tg mice). hemi, hemizygous *MYCN* Tg mice; homo, homozygous *MYCN* Tg mice.

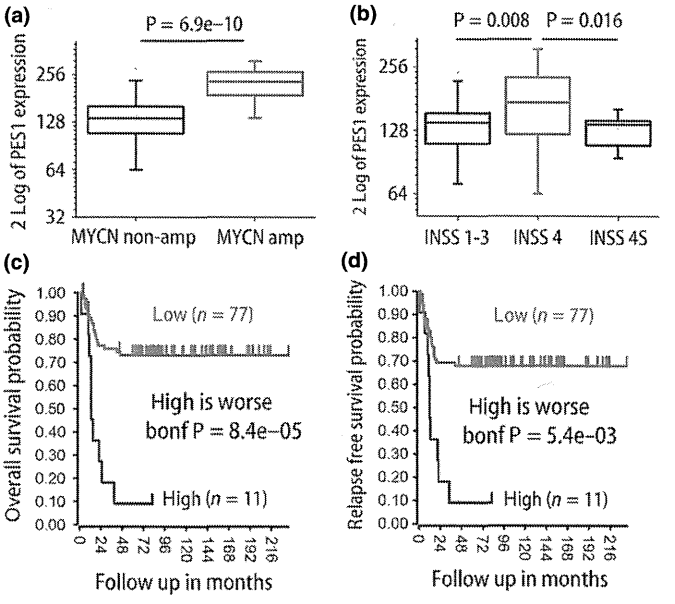

Fig. 2. *PES1* expression in human neuroblastoma cases and patient prognosis (AMC cohort, GSE16476). (a) *PES1* expression in *MYCN* non-amplified/amplified cases ($n = 72$, 16 each). (b) *PES1* expression in each International Neuroblastoma Staging System (INSS) stage (INSS 1–3, $n = 36$; INSS 4, $n = 40$; INSS 4S, $n = 12$). (c,d) Kaplan–Meier curves and log–rank test for overall survival (c) and relapse-free survival (d). Bonf, after Bonferroni correction.

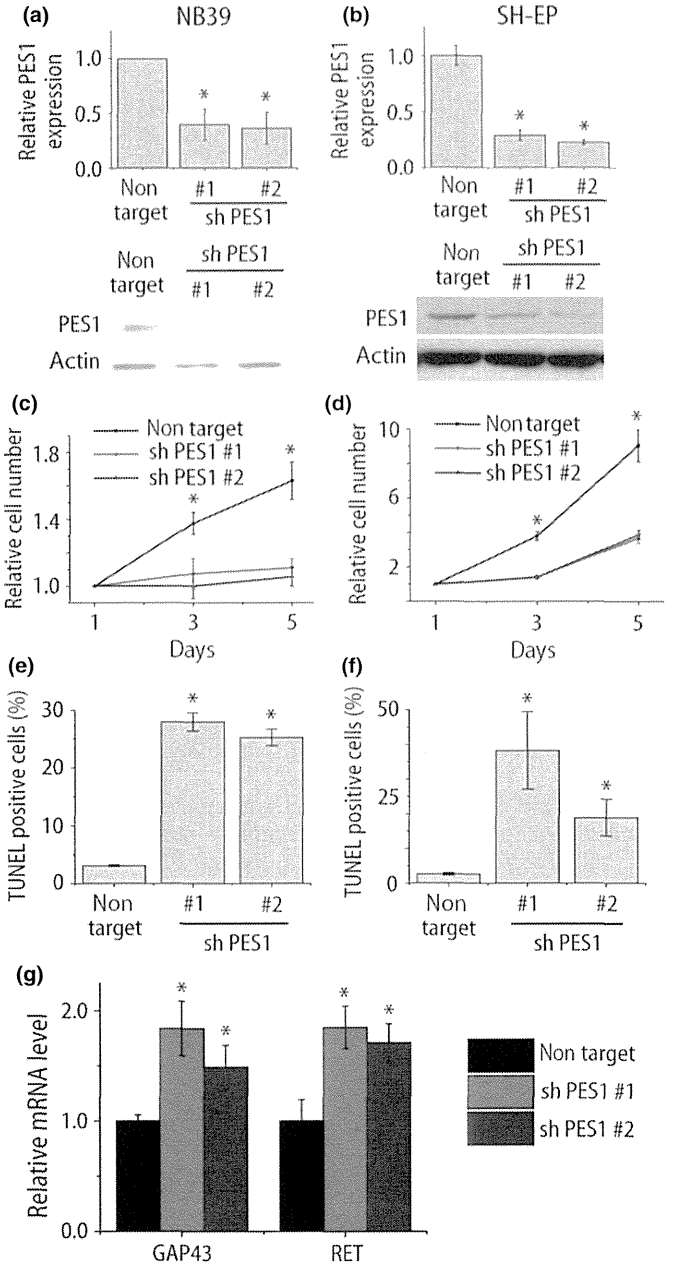

Fig. 3. *PES1* knockdown inhibited neuroblastoma (NB) cell growth and induced apoptosis. (a,b) Quantitative RT-PCR analysis and Western blot analysis of PES1 expression in NB cell lines (NB39 and SH-EP) after shRNA treatments ($n = 3$). (c,d) Cell proliferation analysis of NB cell lines after treatment of non-target shRNA or shRNA against *PES1* (NB39, $n = 4$; SH-EP, $n = 3$). (e,f) Quantification of TUNEL-positive apoptotic cells ($n = 3$). (g) Quantitative RT-PCR analysis of differentiation-related gene expressions of NB39 ($n = 4$). $^*P < 0.05$ non-target versus shRNA against *PES1* (Student's *t*-test).

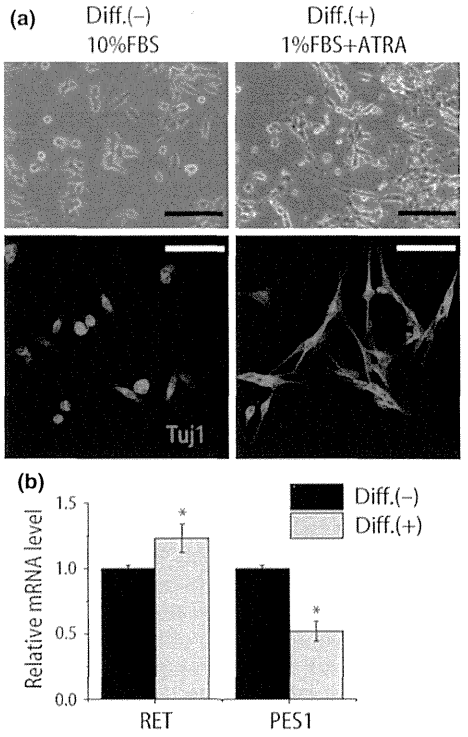

Fig. 4. Induced differentiation attenuated *PES1* expression in neuroblastoma cell line. (a) Phase contrast images (top panels) and confocal image of fluorescence immunostaining for β-tubulin (Tuj1) (red, bottom panels) of NB39 cells under normal culture conditions (10% FBS; Diff.(−)) and differentiation conditions (1% FBS + 1 μM all-trans retinoic acid [ATRA]; Diff.(+)). Hoechst 33258 was used to visualize nuclei. Scale bar = 100 μm. (b) Quantitative RT-PCR analysis of differentiation-related gene (*RET*) and *PES1* expressions ($n = 4$). $^*P < 0.05$ normal culture conditions versus differentiation conditions (Student's *t*-test).

(data not shown), the results of quantitative PCR showed an increase in the expression of differentiation-related genes (Fig. 3g). As the cell shape was not remarkably changed, we could not conclude that *PES1* knockdown caused the differentiation. But this result raised the possibility that *PES1* expression is associated with differentiation status.

Differentiation induction in NB cell lines decreased *PES1* expression. We then examined whether the induction of differentiation can change the *PES1* expression. Historically, various methods have been used to induce NB differentiation, including serum starvation and treatment with all-trans retinoic acid (ATRA).[28–31] A derivative of vitamin A, ATRA is essential for development and differentiation. All-trans retinoic acid-induced differentiation of leukemic cells has been shown to dramatically improve the prognosis of patients with acute promyelocytic leukemia.[32] In addition, ATRA can differentiate NB cells. We induced differentiation in NB cell lines with serum reduction (from 10% FBS in original culture to 1%) and ATRA (1 μM). This treatment increased the number and length of the neuritic extensions of NB39 and TNB1 cells (Fig. 4a, Fig. S2), and these neurites were positive for Tuj1, a neuronal marker. This differentiation induction was further verified by the increased expression of a differentiation-related gene (Fig. 4b, Fig. S2).[33] Interestingly, the differentiation induction decreased *PES1* expression (Fig. 4b, Fig. S2). This result suggests the possibility that ATRA-induced differentiation modulates *PES1* expression.

Differentiation induction in mouse NB model also decreased *PES1* expression. To further verify the association of *PES1* with tumor cell differentiation, we tried another NB model. We used tumorspheres derived from an *MYCN* Tg mouse primary tumor.[21] Differentiation induction with NGF, NT3, and N2 supplement caused radial neurite outgrowth (Fig. 5a). Concurrently, the expressions of differentiation marker (Tuj1) increased and stemness markers (Snail and Musashi) decreased (Fig. 5b). In line with the results in the NB cell lines, *Pes1* expression was reduced with the differentiation induction

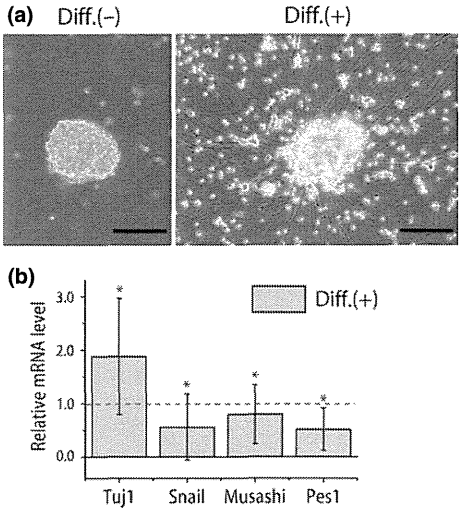

Fig. 5. Induced differentiation decreased *Pes1* expression in *MYCN* transgenic (Tg) mice model tumorsphere. (a) Phase contrast images of tumorspheres established from *MYCN* Tg mice primary tumor under normal culture conditions and differentiation conditions (NGF, NT3 addition). Scale bar = 100 μm. (b) Quantitative RT-PCR analysis of differentiation (β-tubulin, Tuj1) or stemness-related gene (*Snail* and *Musashi*) and *Pes1* expressions (n = 4). Only the values of differentiation conditions are shown (normal culture condition = 1.0). The result is the average of four independently established tumorsphere samples. *$P < 0.05$ normal culture conditions versus differentiation conditions (Student's t-test).

(Fig. 5b). These results suggest that *Pes1* expression was negatively correlated with the differentiation conditions in two kinds of different NB models.

PES1 localized in DFC in nucleolus and DNA damage induced redistribution. As previously reported, PES1 was localized in the nucleolus within the nucleus, where ribosome neogenesis takes place.[9,11] As one of the major roles of PES1 is 32S pre-rRNA processing,[10,34] this distribution is reasonable. The nucleolus consists of three distinct subnucleolar compartments called the fibrillar center, the DFC, and the granular component (GC) from inside to outside,[35] and ribosome maturation also proceeds from inside to outside. A previous analysis using tagged PES1 showed its GC distribution.[11] However, we found that endogenous PES1 is surrounded by nucleolin, a major nucleolar protein that is found in DFC and GC,[36] with nucleolin showing "donut-like" fluorescence (Fig. 6a). Considering the fact that pre-rRNA resides in the DFC, this result suggest that PES1 is mainly localized in DFC of the nucleolus, not in the GC.

In addition to its principal role, ribosome neogenesis, the nucleolus also works as a stress sensor of DNA damage.[37,38] A previous report found that *PES1* knockdown induced the expression of phosphorylated H2AX (γH2AX), a DNA damage marker, and delayed the recovery from DNA damage.[39] The authors indicated some association between PES1 and DNA damage response, but the relationship is still unclear. Therefore, we next investigated the dynamics of PES1 under DNA damage. Camptothecin is a topoisomerase-1 inhibitor that causes DNA damage and is used to treat cancers.[37,40] In the interphase TNB1 cells, PES1 is located in the nucleolus. After treatment with CPT (1 μM) for 5 h, γH2AX was expressed strongly in the nucleus and formed γH2AX foci (Fig. 6b).[41] PES1, together with nucleolin, showed a radical change in distribution to a diffuse nucleoplasmic distribution (Fig. 6b,c). As DNA-damaging agents are known to cause nucleolar disruption,[42] this result was not surprising. The reason for this distribution change and its biological significance remains to be investigated. This result suggests that DNA damage can redistribute PES1 as well as nucleolin. PES1 expression partially, but not completely, overlapped with γH2AX (Fig. 6d).

Discussion

The present study addressed the roles of PES1 in NB tumorigenesis by using a clinical NB database of mRNA expression and survival, human NB cell lines, an NB model in MYCN Tg mice, and tumorspheres derived from *MYCN* Tg mice. *MYCN*

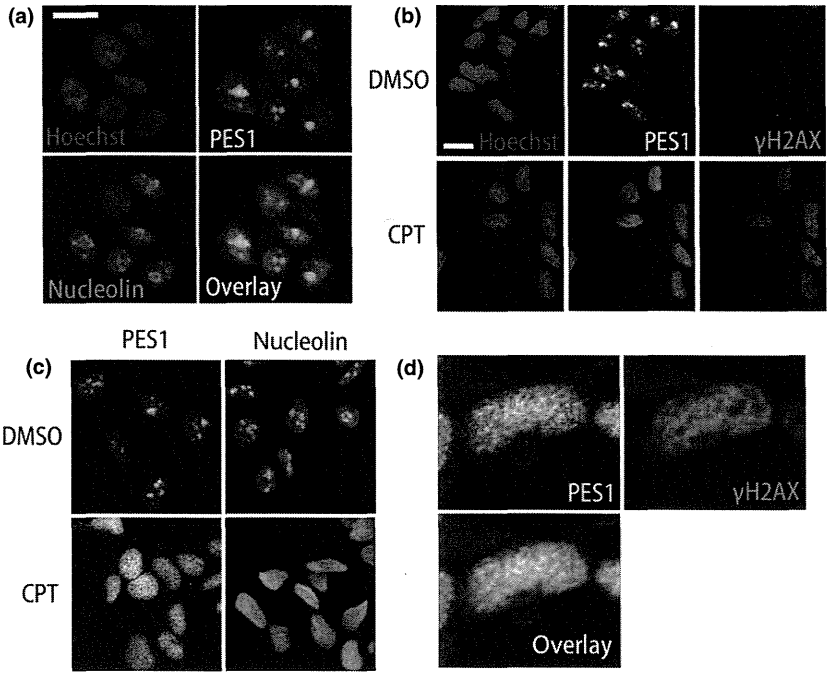

Fig. 6. Endogenous PES1 localization and its redistribution after DNA damage. (a) Confocal images of TNB1 neuroblastoma cells immunostained for PES1 (green) and nucleolin (red) with nuclear stain (Hoechst33258, blue). PES1 is encircled by nucleolin, which shows "donut-like" staining. (b,c) Confocal images of TNB1 cells after DMSO or camptothecin (CPT; 1 μM) treatment. Scale bar = 15 μm. (d) Enlarged confocal images of TNB1 cells after CPT (1 μM) treatment. One nucleus was enlarged.

Tg mice are a reliable NB model that recapitulates the clinical features of NB, histology, and molecular changes.[17,43] Our study revealed that PES1 is involved in NB cell growth, survival, and differentiation. Its high expression is associated with poor prognosis. *PES1* knockdown suppresses NB tumor cell growth and induces apoptosis. In their differentiated state, the NB cell lines and tumorspheres show lower *PES1* expression. In contrast, *PES1* knockdown induces differentiation features. In addition, we found PES1 distribution in DFC in the nucleolus and diffuse redistribution into the nucleoplasm after CPT treatment.

Our study showed that *PES1* is a prognostic marker of NBs. Neuroblastoma cases with unfavorable prognosis (*MYCN* amplified or INSS 4) show high *PES1* expression. Previous reports indicated that cancerous tissue expressed more *PES1* than normal tissue or benign tumors.[9,14–16,26] However, these results were based on the results of tissue microarray or cell lines. We showed the relationship between *PES1* expression and prognosis in NBs in this study for the first time. As previously shown in colon cancer cell lines,[26] PES1 knockdown strikingly suppressed NB cell growth in our study.

We showed that *PES1* knockdown upregulated some differentiation-related genes. To further elucidate the relationship between *PES1* expression and differentiation, we used two different kinds of models to induce NB differentiation. One is ATRA treatment of NB cell lines, and the other is tumorsphere differentiation with growth factors. We previously reported a new tumorsphere culture condition,[21] and found that this condition worked well in the present experimental scheme. In both models, we successfully induced differentiation as demonstrated by morphology change (neurite growth) and differentiation marker expression. Under these conditions, *PES1* was downregulated. However, we could not successfully rescue these phenomena by *PES1* overexpression (data not shown). These results suggest that PES1 is required but not sufficient to suppress NB cell differentiation.

We also reanalyzed PES1 distribution in the nucleoli using confocal microscopy. In our analysis, PES1 was encircled by nucleolin. Nucleolin and nucleophosmin are the two major protein components of the nucleolus. Previous reports have described multiple functions of nucleolin from rRNA splicing to ribosome assembly. Our results indicate that PES1 is mainly distributed in DFC, but not GC, whereas nucleolin is localized in DFC and GC. As DFC is an rRNA-rich lesion in nucleoli, the DFC distribution of PES1 makes sense. We also observed a dynamic change of PES1 distribution after treatment with the DNA-damaging agent CPT. The relationship between PES1 and DNA damage response is still unclear. One previous study indicated that PES1 works protectively against DNA damage and PES1 knockdown induces γH2AX expression.[39] From our results and previous knowledge, we can hypothesize that *PES1* knockdown causes DNA damage and accumulated DNA damage drives cells to apoptosis.

Another interesting fact is that PES1 has been known to have a BRCA1 C-terminal domain (BRCT domain).[12] The BRCT domain is a phosphoprotein binding domain and an integral signaling module in the DNA damage response.[44] As the role or binding partners of the BRCT domain of PES1 is not known, we investigated the binding partners of PES1 using liquid chromatography–mass spectrometry with peptide mass fingerprinting (LC-MS/MS). At this stage, NONO and SFPQ are among the list of identified proteins as binding partners (data not shown). These proteins form heterodimers and enhance DNA strand break rejoining.[45,46] These results also suggested the possible close association of PES1 with DNA damage. But we need further study to elucidate the role of PES1 in DNA damage response.

In this article, we described multiple functions of the PES1 protein. The classical and best-known role of PES1 is ribosome genesis.[10,11]. The ribosome is an essential intracellular organelle to protein synthesis, and its dysfunction cause severe cellular disturbance. The growth inhibitions and apoptosis observed in our study (Fig. 3) might be caused by this ribosomal dysfunction. In addition, as mentioned above, DNA damage caused by *PES1* knockdown could also be the cause of apoptosis and growth inhibitions. Arrest of cell division is a prerequisite to enter a program of differentiation.[47] Therefore, the phenotypes related to differentiation (Figs. 3–5) are closely linked to growth inhibition.

In summary, we showed that PES1 is a good prognostic marker of NBs. As a multifunctional protein, PES1 is involved in NB cell survival and differentiation. DNA damage might contribute to apoptosis regulation in NB cells.

Acknowledgments

This work was supported in part by a grant-in-aid from the National Cancer Center Research and Development Fund (22-4 to KK) and Health and Labor Sciences Research Expenses for Commission, Applied Research for Innovative Treatment of Cancer (H26-applied-general-006) from the Ministry of Health, Labor and Welfare.

Disclosure Statement

The authors have no conflicts of interest.

References

1 Maris JM, Hogarty MD, Bagatell R, Cohn SL. Neuroblastoma. *Lancet* 2007; **369**: 2106–20.
2 Kocak H, Ackermann S, Hero B *et al.* Hox-C9 activates the intrinsic pathway of apoptosis and is associated with spontaneous regression in neuroblastoma. *Cell Death Dis* 2013; **4**: e586.
3 Matthay KK, Villablanca JG, Seeger RC *et al.* Treatment of high-risk neuroblastoma with intensive chemotherapy, radiotherapy, autologous bone marrow transplantation, and 13-cis-retinoic acid. Children's Cancer Group. *N Engl J Med* 1999; **341**: 1165–73.
4 Maris JM, Matthay KK. Molecular biology of neuroblastoma. *J Clin Oncol* 1999; **17**: 2264–79.
5 Guglielmi L, Cinnella C, Nardella M *et al.* MYCN gene expression is required for the onset of the differentiation programme in neuroblastoma cells. *Cell Death Dis* 2014; **5**: e1081.
6 Allende ML, Amsterdam A, Becker T, Kawakami K, Gaiano N, Hopkins N. Insertional mutagenesis in zebrafish identifies two novel genes, pescadillo and dead eye, essential for embryonic development. *Genes Dev* 1996; **10**: 3141–55.
7 Simmons T, Appel B. Mutation of pescadillo disrupts oligodendrocyte formation in zebrafish. *PLoS ONE* 2012; **7**: e32317.
8 Gessert S, Maurus D, Rossner A, Kuhl M. Pescadillo is required for Xenopus laevis eye development and neural crest migration. *Dev Biol* 2007; **310**: 99–112.
9 Kinoshita Y, Jarell AD, Flaman JM *et al.* Pescadillo, a novel cell cycle regulatory protein abnormally expressed in malignant cells. *J Biol Chem* 2001; **276**: 6656–65.
10 Du YC, Stillman B. Yph1p, an ORC-interacting protein: potential links between cell proliferation control, DNA replication, and ribosome biogenesis. *Cell* 2002; **109**: 835–48.
11 Oeffinger M, Leung A, Lamond A, Tollervey D. Yeast Pescadillo is required for multiple activities during 60S ribosomal subunit synthesis. *RNA* 2002; **8**: 626–36.

12 Holzel M, Grimm T, Rohrmoser M *et al.* The BRCT domain of mammalian Pes1 is crucial for nucleolar localization and rRNA processing. *Nucleic Acids Res* 2007; **35**: 789–800.
13 Grimm T, Holzel M, Rohrmoser M *et al.* Dominant-negative Pes1 mutants inhibit ribosomal RNA processing and cell proliferation via incorporation into the PeBoW-complex. *Nucleic Acids Res* 2006; **34**: 3030–43.
14 Weber A, Hengge UR, Stricker I *et al.* Protein microarrays for the detection of biomarkers in head and neck squamous cell carcinomas. *Hum Pathol* 2007; **38**: 228–38.
15 Kim B, Bang S, Lee S *et al.* Expression profiling and subtype-specific expression of stomach cancer. *Cancer Res* 2003; **63**: 8248–55.
16 Li J, Yu L, Zhang H *et al.* Down-regulation of pescadillo inhibits proliferation and tumorigenicity of breast cancer cells. *Cancer Sci* 2009; **100**: 2255–60.
17 Weiss WA, Aldape K, Mohapatra G, Feuerstein BG, Bishop JM. Targeted expression of MYCN causes neuroblastoma in transgenic mice. *EMBO J* 1997; **16**: 2985–95.
18 Murakami-Tonami Y, Kishida S, Takeuchi I *et al.* Inactivation of SMC2 shows a synergistic lethal response in MYCN-amplified neuroblastoma cells. *Cell Cycle* 2014; **13**: 1115–31.
19 Lutz W, Stohr M, Schurmann J, Wenzel A, Lohr A, Schwab M. Conditional expression of N-myc in human neuroblastoma cells increases expression of alpha-prothymosin and ornithine decarboxylase and accelerates progression into S-phase early after mitogenic stimulation of quiescent cells. *Oncogene* 1996; **13**: 803–12.
20 Kishida S, Mu P, Miyakawa S *et al.* Midkine promotes neuroblastoma through Notch2 signaling. *Cancer Res* 2013; **73**: 1318–27.
21 Cao D, Kishida S, Huang P *et al.* A new tumorsphere culture condition restores potentials of self-renewal and metastasis of primary neuroblastoma in a mouse neuroblastoma model. *PLoS ONE* 2014; **9**(1): e86813.
22 Huang P, Kishida S, Cao D *et al.* The neuronal differentiation factor NeuroD1 downregulates the neuronal repellent factor Slit2 expression and promotes cell motility and tumor formation of neuroblastoma. *Cancer Res* 2011; **71**: 2938–48.
23 Hansford LM, Thomas WD, Keating JM *et al.* Mechanisms of embryonal tumor initiation: distinct roles for MycN expression and MYCN amplification. *Proc Natl Acad Sci USA* 2004; **101**: 12664–9.
24 Brodeur GM, Pritchard J, Berthold F *et al.* Revisions of the international criteria for neuroblastoma diagnosis, staging, and response to treatment. *J Clin Oncol* 1993; **11**: 1466–77.
25 Monclair T, Brodeur GM, Ambros PF *et al.* The International Neuroblastoma Risk Group (INRG) staging system: an INRG Task Force report. *J Clin Oncol* 2009; **27**: 298–303.
26 Xie W, Feng Q, Su Y *et al.* Transcriptional regulation of PES1 expression by c-Jun in colon cancer. *PLoS ONE* 2012; **7**: e42253.
27 Matsushima H, Bogenmann E. Expression of trkA cDNA in neuroblastomas mediates differentiation in vitro and in vivo. *Mol Cell Biol* 1993; **13**: 7447–56.
28 Seidman KJ, Barsuk JH, Johnson RF, Weyhenmeyer JA. Differentiation of NG108-15 neuroblastoma cells by serum starvation or dimethyl sulfoxide results in marked differences in angiotensin II receptor subtype expression. *J Neurochem* 1996; **66**: 1011–18.
29 Hill DP, Robertson KA. Characterization of the cholinergic neuronal differentiation of the human neuroblastoma cell line LA-N-5 after treatment with retinoic acid. *Brain Res Dev Brain Res* 1997; **102**: 53–67.
30 Huang S, Laoukili J, Epping MT *et al.* ZNF423 is critically required for retinoic acid-induced differentiation and is a marker of neuroblastoma outcome. *Cancer Cell* 2009; **15**: 328–40.
31 Frumm SM, Fan ZP, Ross KN *et al.* Selective HDAC1/HDAC2 inhibitors induce neuroblastoma differentiation. *Chem Biol* 2013; **20**: 713–25.
32 Fenaux P, Chastang C, Chomienne C *et al.* Treatment of newly diagnosed acute promyelocytic leukemia (APL) by all transretinoic acid (ATRA) combined with chemotherapy: the European experience. European APL Group. *Leuk Lymphoma* 1995; **16**: 431–7.
33 Celay J, Blanco I, Lazcoz P, Rotinen M, Castresana JS, Encio I. Changes in gene expression profiling of apoptotic genes in neuroblastoma cell lines upon retinoic acid treatment. *PLoS ONE* 2013; **8**: e62771.
34 Lapik YR, Fernandes CJ, Lau LF, Pestov DG. Physical and functional interaction between Pes1 and Bop1 in mammalian ribosome biogenesis. *Mol Cell* 2004; **15**(1): 17–29.
35 Raska I, Shaw PJ, Cmarko D. Structure and function of the nucleolus in the spotlight. *Curr Opin Cell Biol* 2006; **18**: 325–34.
36 Ugrinova I, Monier K, Ivaldi C *et al.* Inactivation of nucleolin leads to nucleolar disruption, cell cycle arrest and defects in centrosome duplication. *BMC Mol Biol* 2007; **8**: 66.
37 Rubbi CP, Milner J. Disruption of the nucleolus mediates stabilization of p53 in response to DNA damage and other stresses. *EMBO J* 2003; **22**: 6068–77.
38 Bernardi R, Scaglioni PP, Bergmann S, Horn HF, Vousden KH, Pandolfi PP. PML regulates p53 stability by sequestering Mdm2 to the nucleolus. *Nat Cell Biol* 2004; **6**: 665–72.
39 Xie W, Qu L, Meng L, Liu C, Wu J, Shou C. PES1 regulates sensitivity of colorectal cancer cells to anticancer drugs. *Biochem Biophys Res Commun* 2013; **431**: 460–5.
40 Buckwalter CA, Lin AH, Tanizawa A, Pommier YG, Cheng YC, Kaufmann SH. RNA synthesis inhibitors alter the subnuclear distribution of DNA topoisomerase I. *Cancer Res* 1996; **56**: 1674–81.
41 Riballo E, Kuhne M, Rief N *et al.* A pathway of double-strand break rejoining dependent upon ATM, Artemis, and proteins locating to gamma-H2AX foci. *Mol Cell* 2004; **16**: 715–24.
42 Boulon S, Westman BJ, Hutten S, Boisvert FM, Lamond AI. The nucleolus under stress. *Mol Cell* 2010; **40**: 216–27.
43 Kiyonari S, Kadomatsu K. Neuroblastoma models for insights into tumorigenesis and new therapies. *Expert Opin Drug Discov* 2015; **10**(1): 53–62.
44 Leung CC, Glover JN. BRCT domains: easy as one, two, three. *Cell Cycle* 2011; **10**: 2461–70.
45 Krietsch J, Caron MC, Gagne JP, Ethier C, Vignard J, Vincent M, *et al.* PARP activation regulates the RNA-binding protein NONO in the DNA damage response to DNA double-strand breaks. *Nucleic Acids Res* 2012; **40**: 10287–301.
46 Salton M, Lerenthal Y, Wang SY, Chen DJ, Shiloh Y. Involvement of Matrin 3 and SFPQ/NONO in the DNA damage response. *Cell Cycle* 2010; **9**: 1568–76.
47 Peunova N, Enikolopov G. Nitric oxide triggers a switch to growth arrest during differentiation of neuronal cells. *Nature* 1995; **375**: 68–73.

Supporting Information

Additional supporting information may be found in the online version of this article:

Fig. S1. MYCN induction in MYCN single-copy cell lines.

Fig. S2. Induced differentiation in TNB1 neuroblastoma cells.

Table S1. Short hairpin RNA target sequences (PES1).

Table S2. Primer sequences for PCR experiments.

OPEN ACCESS Freely available online

PLOS | ONE

A New Tumorsphere Culture Condition Restores Potentials of Self-Renewal and Metastasis of Primary Neuroblastoma in a Mouse Neuroblastoma Model

Dongliang Cao[1], Satoshi Kishida[1], Peng Huang[1], Ping Mu[1], Shoma Tsubota[1], Masaaki Mizuno[2], Kenji Kadomatsu[1]*

1 Department of Biochemistry, Nagoya University Graduate School of Medicine, Nagoya, Japan, **2** Center for Advanced Medicine and Clinical Research, Nagoya University Hospital. Nagoya, Japan

Abstract

Tumorsphere culture enriches and expands tumor cells, thus providing important resources for cancer studies. However, as compared with metastatic tissues, primary tumors in the nervous system rarely give rise to long-surviving tumorspheres, thereby seriously limiting studies on these cancers. This might be due to the limited self-renewal capability of tumor cells and/or to inappropriate culture conditions. The growth and maintenance of tumor cells may depend on microenvironments and/or cell origins (e.g., primary or metastatic; stem cell-like or progenitor-like). Here, we attempted to establish a tumorsphere culture condition for primary neuroblastoma (NB). Primary tumors in *MYCN* transgenic mice, a NB model, could be serially transplanted, suggesting that these tumors contain cells with a high self-renewal potential. However, primary tumors did not give rise to tumorspheres under a serum-free neurosphere culture condition. The newly established culture condition (named PrimNeuS) contained two critical ingredients: fetal bovine serum and β-mercaptoethanol were essential for tumorsphere formation as well as indefinite passages. The spheres could be passaged more than 20 times without exhaustion under this condition, exhibited a property of differentiation and formed tumors *in vivo*. Unexpectedly, PrimNeuS revealed that the *MYCN* transgenic mice had bone marrow metastasis. Furthermore, subcutaneous tumors derived from tumorspheres of primary tumors showed bone marrow metastasis. Taken together, PrimNeuS provides resources for the study of NB and can be used as a powerful tool for the detection of minimal residual disease and for *in vitro* evaluation prior to personalized therapy.

Citation: Cao D, Kishida S, Huang P, Mu P, Tsubota S, et al. (2014) A New Tumorsphere Culture Condition Restores Potentials of Self-Renewal and Metastasis of Primary Neuroblastoma in a Mouse Neuroblastoma Model. PLoS ONE 9(1): e86813. doi:10.1371/journal.pone.0086813

Editor: Zhongjun Zhou, The University of Hong Kong, Hong Kong

Received March 29, 2013; **Accepted** December 19, 2013; **Published** January 22, 2014

Funding: This work was supported in part by a grant-in-aid from the National Cancer Center Research and Development Fund (22-4 to KK; http://www.cancer.gov/cancertopics/factsheet/NCI/NCI); by a Grant-in-Aid for Scientific Research on Innovative Areas (23110002 to KK) from the Ministry of Education, Culture, Sports, Science, and Technology (MEXT) of Japan (http://www.molecular-activation.jp/index_e.html); by Grants-in-Aid from MEXT (23390078 to KK; 24590377 to SK); Grant-in-Aid for Scientific Research on Innovative Areas to MM. The funders had no role in study design, data collection and analysis, decision to publish, or preparation of the manuscript.

Competing Interests: The authors have declared that no competing interests exist.

* E-mail: kkadoma@med.nagoya-u.ac.jp

Introduction

Tumorsphere culture provides important resources for cancer studies, since it enriches and expands tumor cells. However, the efficiency with which long-surviving tumorspheres are established from primary tumors in the nervous system is not satisfactory, whereas tumorspheres are obtained from metastatic tissues with relative ease. For example, only half of primary high-grade gliomas are able to give rise to tumorsphere lines [1]. Low-grade gliomas rarely give rise to tumorspheres. It is also hard to obtain tumorsphere lines from primary neuroblastomas (NBs), in contrast to those from metastatic tumors [2]. These low efficiencies of tumorsphere formation from primary tumors seriously limit studies on these cancers.

Tumor cells *in vivo* may reside in a microenvironment suitable for maintenance and growth. Such microenvironments may differ between tumor types and origins, e.g., primary or metastatic; stem cell-like or progenitor-like. This may be why a common protocol for tumorsphere cultures cannot be established. Therefore, if appropriate conditions were provided, tumorspheres could be grown *in vitro*. We addressed this hypothesis in the present study by employing *MYCN* transgenic mice, a NB model.

NB is the most common pediatric extracranial solid tumor and is derived from sympathetic neurons [3]. Despite intensive multimodal therapy, high-risk NB patients with relapse in bone marrow have less than a 10% chance of survival [4]. To overcome this problem, it is particularly important to verify the mechanisms of tumor initiation and the metastasis of NB, which remain elusive.

Here, we have established culture condition for long-surviving tumorspheres from primary NBs. This culture condition restores the potential for self-renewal and metastasis of primary NBs.

Materials and Methods

Ethics Statement

This study was carried out in strict accordance with the recommendations in the Guide for the Care and Use of Laboratory Animals of the National Institutes of Health. This

study was approved by the Animal Care and Use Committee of Nagoya University Graduate School of Medicine (Permit Number: 24371). All efforts were made to minimize suffering.

Primary Culture of Tumorspheres from Allograft Tumors and Primary Tumors of *MYCN* Transgenic Mice

The procedure was similar to that used in a previous report [5]. Briefly 0.5-cm^3 of tumor tissue was dissected from an allograft tumor of 25 generations or from a primary tumor of *MYCN* transgenic mice. After washing, the tissue was minced and digested with 0.25% trypsin (Sigma) for 15 minutes, and the digestion was stopped by adding trypsin inhibitor (Sigma). The cells were centrifuged and washed twice. The supernatant was collected into a new tube and centrifuged. To eliminate the red blood cells, the pellet was treated with RBC lysis buffer (Biolegend) according to the manufacturer's instructions. The cells were then ready for culture. To get tumorspheres from allograft tumors, cells were cultured as previously reported, with DMEM/F12ham (Sigma) plus EGF 10 ng/ml, bFGF 15 ng/ml (Peprotech), 2% B27 supplement, and 1% penicillin/streptomycin (PS, GIBCO), which can be called medium #1. To get tumorspheres from the primary tumors, some other medium cocktails were investigated: medium #2, DMEF/F12ham, 15% FBS (Hyclone), 2% B27 supplement, 1% PS; medium #3, medium #1 plus 15% FBS; medium #4 [6,7], medium #3 plus 1% non-essential amino acid (NEAA), 1% sodium pyruvate, 55 μM β-mercaptoethanol [8]; medium #5 is medium #4 without FBS; and medium #6 is medium #4 without β-mercaptoethanol. Cells were cultured in a nontreated petri dish in a 37°C, 5% CO_2 tissue culture incubator. Successfully formed tumorspheres were digested with trypsin and dissociated into single cells by pipetting with a 1 ml tip and were passed every 3–4 days.

Tumorsphere Growth Assay

The self-renewal ability of tumorspheres was evaluated by clonogenic assay. Cells were dissociated by trypsin treatment and filtered through a 70 μm nylon mesh, then stained with trypan blue. The viable cells were counted with a hemocytometer under a microscope, and 1000 cells were seeded into 24-well nontreated petri dish. Five days later, the spheres were counted. For sphere size, pictures were taken under a phase-contrast microscope. The sphere diameter was measured by Metamorph 6.1 software (Molecular Devices); 100 randomly selected tumorspheres were measured for each group if possible. To perform a proliferation assay, 10^5 dissociated cells were seed into a 6 cm petri dish. Five days later, the spheres were dissociated into single cells and stained with trypan blue. The viable cells were counted.

To evaluate the enrichment of the stem cells with the new condition, the sphere-forming potential of both the tumor cells of *MYCN* hemizygous transgenic mice and the tumorsphere cells passaged 4 times in the new condition was checked by ELDA (extreme limiting dilution analysis) [9]. Briefly, after dissociation cells were seeded in a 96 well-plate at a density of 640, 320, 160, 80, 40, 20, 10 or 5 cells/well in 200 μl culture medium (6 wells per group). Another 100 μl medium was added 3 days later. At one week, spheres in each well were counted, and the sphere-forming potential was calculated following the instruction of ELDA.

Induced Differentiation of Tumorspheres and Immunofluorescence Staining

Spheres were collected at low centrifuge speed, about 300–400 rpm, and were washed once to remove dead cell debris. They were then re-suspended with medium containing DMEM/F12ham, 1% FBS, 2% B27 supplement, 1% sodium pyruvate, 10^3 units/ml LIF, and 1% PS. The spheres were seeded into poly-D-lysine/laminin/fibronectin pre-coated four-well chamber slides (BD). After 12 hours, the medium was changed to differentiation medium: DMEM/F12ham, 1% FBS, 2% B27 supplement, 1% N2 supplement, 50 ng/ml NGF, 50 ng/ml NT3 and 1% PS. The medium was changed everyday. After 3 days, differentiated cells were fixed and checked by immunofluorescence staining.

In vivo Assays of Tumorigenicity and Immunohistochemistry

First, 10^4 sphere cells were mixed with PBS containing 30% Matrigel (BD Biosciences) and subcutaneously inoculated into 1-month-old 129/SVJ WT mice in both flanks. Three weeks later, the tumors were dissected and weighed. The tumor volume was measured every week using a digital caliper. Volume was calculated as $V = \text{height} \times \text{width}2/2$. To compare the tumor formation potential, the primary tumor cells, the corresponding primary tumor sphere cells, allograft tumor cells and the corresponding allograft tumor sphere cells were injected subcutaneously into 4 to 5 week-old wild-type mice at different cell numbers, that is 10^4, 10^3, 10^2, 10 cells/200 μl 30% matrigel, and investigated for 1.5 months to evaluate the potential. For histological evaluation, tissues were fixed in 4% paraformaldehyde, dehydrated and embedded in paraffin according to the standard procedure. The samples were cut into 5 μm sections and stained with hematoxylin and eosin for routine checks. After deparaffinage, immunohistochemistry was carried out by blocking endogenous peroxidase activity and then incubating antigen retrieval sections with anti-TH (CHEMICON, AB125), Sox2 (Abcam, ab97957), or Pax6 (Abcam, ab5790) overnight at 4°C following incubation with biotin-conjugated goat anti-rabbit or anti-mouse secondary antibody (BD Pharmingen) for 30 minutes at room temperature. Signals were amplified using the Vectorstain ABC kit (Vector Laboratories) and detected by DAB (Dako) following the manufacturers' instructions.

Evaluation of Bone Marrow Metastasis

Tumorsphere cells were dissociated into single cells and transfected with EF-promoter-Venus vector through lentivirus. The virus was packaged as previously reported [5]. After FACS sorting, the cells were passaged twice *in vitro* and then 10^5 cells were inoculated into syngenic 129/Svj wild type mice. 6 weeks later, the bone marrow cells from both femoral bones were collected, and dissociated into single cell suspension with 25G needles and filtered through 70 μm nylon mesh. The cells were then cultured under the new condition. To examine metastasis of *MYCN* transgenic mice, 3-month-old wild type and hemizygous mice were sacrificed and the bone marrow cells were cultured with a method as described above.

Total RNA Extraction and RT-PCR

Total RNA was extracted by the Total RNA Extraction Miniprep System Kit (VioGene Biosciences) following the manufacturer's instructions. After DNaseI treatment, the same amount of RNA was reverse-transcribed into cDNA with the ReverTra Ace qPCR® RT Kit (TOYOBO). Real-time PCR reaction was carried out with the Thunderbird SYBR qPCR Mix kit (TOYOBO) on Stratagene Mx3005P system. The primers used are listed in Table 1.

Table 1. Primers used in PCR experiments.

	Forward	Reverse
TH	cagagttggataagtgtcaccac	gggtagcatagaggcccttca
Hand2	tcaacagcgccttcgccgagct	ttgtcgttgctgctcactgtgc
Phox2b	gaccaccagagcagtccgtacg	agtgctgtcgggatcagtgctc
Phox2a	caattcgtacgattcgtgcgtg	acctgcacgcgagcctcagtga
NPY	tggactgaccctcgctctat	gatgagggtggaaacttgga
SYP	ctcctcggctgaattctttg	acagggtccctcagttcctt
Musashi	atggtggaatgcaagaaagc	taggtgtaaccaggggcaag
Sox2	ctctgcacatgaaggagcac	atgtaggtctgcgagctggt
Pax6	agttcttcgcaacctggcta	gaagtcgcatctgagcttcat
C-myc	gcccagtgaggatatctgga	atcgcagatgaagctctggt
Klf4	ccaaagaggggaagaaggtc	agtgcctggtcagttcatcg
Oct3/4	cacgagtggaaagcaactca	agatggtggtctggctgaac
Snail	gaggacagtggcaaaagctc	ggagaatggcttctcaccag
GAPDH	ggaggccatgtaggccatga	ggtggtgaagcaggcatctg

doi:10.1371/journal.pone.0086813.t001

Statistical Analysis of Data

Statistical significance was evaluated by the two-tailed Student's t-test. $P<0.05$ was considered to indicate a significant difference. Results are expressed as means±SD.

Results

Traditionally, tumorspheres from nervous system tumors have been cultured in serum-free conditions developed to support normal neural stem cells (NSCs) [10]. Normal NSCs expand when cultured under neurosphere culture conditions, but normal progenitors typically do not [11]. Indeed, a serum-free neurosphere culture condition works well to form tumorspheres from metastatic bone marrow tissues of human NBs [2].

Serial xenotransplantation can increase the population of TICs [12,13]. We previously established an allograft tumor model by serially allografting minced tumors of *MYCN* Tg mice [5]. Tumorspheres were formed and grew rapidly from allograft tumors, but not primary tumors, of *MYCN* Tg mice under a serum-free neurosphere culture condition (Fig. 1A). Tumorspheres from allograft tumors showed no exhaustion after 20 passages (Fig. 1B). However, this culture condition did not support the growth of tumorspheres from primary NBs (Fig. 1A,B).

Next, we sought for a suitable culture condition for tumorspheres from primary NBs. First, we compared four different conditions: #1, serum-free neurosphere medium containing EGF, bFGF and B27; #2, medium containing 15% FBS and B27; #3, #2 plus EGF and bFGF; #4, #3 plus non-essential amino acids (NEAA), sodium pyruvate and β -mercaptoethanol. The #1, #2 and #3 conditions did not support tumorsphere formation from primary NB tissues of *MYCN* Tg mice (Fig. 2A and B, #1-3). In contrast, tumorspheres formed well in the #4 condition (Fig. 2A and B, #4). The #4 medium resembled the medium for pluripotent stem cells, e.g., embryonic stem cells. But leukemia inhibitory factor (LIF) was omitted in this medium, because LIF rather enhanced differentiation and thus inhibited the long-term passage of sphere cells (data not shown).

Next, we asked which ingredients were important in the #4 medium. We found that FBS and β-mercaptoethanol were indispensable for sphere formation and long-term survival. Thus, medium without FBS showed less sphere formation (Fig. 2A and B, #5). This medium did not support indefinite passaging (Fig. 2C, #5). Medium without β-mercaptoethanol did not form spheres (Fig. 2A–C, #6).

We employed ELDA (extreme limiting dilution analysis) [9] to evaluate the sphere-forming potential of both tumor cells freshly prepared from tumors of *MYCN* hemizygous transgenic mice and tumorsphere cells passaged 4 times in #4 medium. We found that about 5 cells freshly isolated from primary tumors could form a sphere, whereas about 2 cells of tumorspheres grown in #4 medium were enough to form a sphere (Fig. 2D). The data suggest that cells with self-renewal capacity were enriched in #4 medium.

Next, we performed a head-to-head comparison of sphere (with a diameter more than 150 μm)-forming efficiency under different culture conditions, i.e., #1 and #4. We did a limited dilution adjusting cell density to 1 to 80 per well and incubated the cells for 7 days. We found that cells cultured in #1 medium did not form spheres, whereas #4 medium supported sphere formation (Fig. 2E). Taking into account that the size of spheres counted was big enough, our data suggest that #4 medium increased the sphere-formation efficiency.

We then compared the properties of sphere cells cultured in #1 and #4 medium and adherent cells. As cells could hardly survive for a long time in #1 medium, we collected all the samples after 3 days culture. As summarized in Fig. 2F, all the NB markers (Hand2, TH, Phox2a, Phox2b and SYP) and the neural crest stem cell marker Musashi tended to increase in sphere cells cultured in #4 medium as compared with sphere cells cultured in #1 medium and adherent cells.

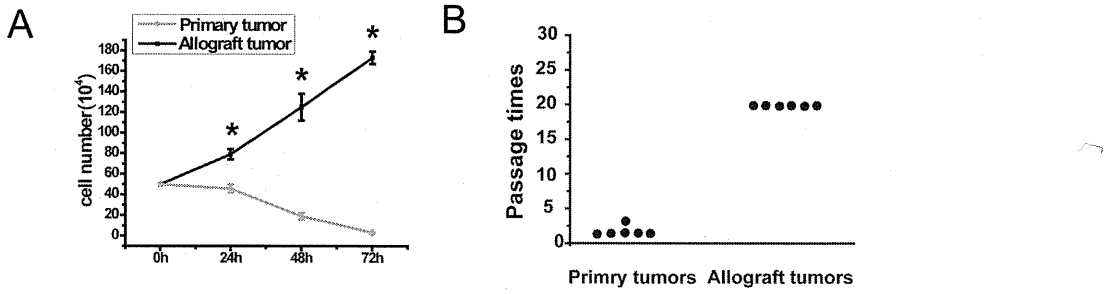

Figure 1. NSC condition can support the long-term survival of tumor cells from allograft tumors but not from primary tumors of MYCN transgenic mice. A, 5×10^5 cells freshly isolated from allograft tumors and primary tumors were cultured under NSC condition. Cells were counted every day. *$P<0.05$. B, Both kinds of cells were passaged every 3 days until exhaustion. Passage was stopped after 20 times.
doi:10.1371/journal.pone.0086813.g001